Development and Test of a GEM-Based TEPC for Neutron Protection Dosimetry

A Dissertation
Presented to
The Academic Faculty

by

Marat Seydaliev

In Partial Fulfillment
of the Requirements for the Degree
Doctor of Philosophy in Nuclear Engineering
The Woodruff School of Mechanical Engineering

Georgia Institute of Technology

May 2007

Development and Test of a GEM-Based TEPC for Neutron Protection Dosimetry

Approved by:

Dr. C-K. Chris Wang, Advisor
School of Mechanical Engineering
Georgia Institute of Technology

Dr. John L. Wood
School of Physics
Georgia Institute of Technology

Dr. Nolan Hertel
School of Mechanical Engineering
Georgia Institute of Technology

Dr. Tim Fox
Emory University

Dr. Cassiano de Oliveira
School of Mechanical Engineering
Georgia Institute of Technology

Date Approved: February, 2 2007

ACKNOWLEDGEMENTS

I would like to acknowledge many people for helping me during my doctoral work. I would especially like to thank my advisor, Dr. Wang, for his generous time and commitment. Throughout my doctoral work he encouraged me to develop problem solving and research skills. He continually stimulated my analytical thinking and greatly assisted me with scientific research.

I am also very grateful for having an exceptional doctoral committee and wish to thank Dr. Wang, Dr. Hertel, Dr. de Olivera, Dr. Wood, and Dr. Fox for their time, encouragement and helpful comments.

I wish to thank Dr. Hertel for allowing me to use ^{252}Cf and AmBe neutron sources.

I am very grateful for the assistance and advice in all the experiments I received from the staff of Georgia Tech Office of Radiation Safety.

I owe a special note of gratitude to Anant Mandapaka for assisting me with miscellaneous tasks in building and testing the new detector.

I extend many thanks to the ME Machine shop manager John Graham, to the Georgia Tech Clean Room manager Gary Spinner and Clean Room staff member Brandon Harrington for their patience and prompt assistance in our needs.

Also I would like to thank DOE for the financial support of this research through the Nuclear Engineering Education Research (NEER) Grant.

Finally, I'd like to thank my family and friends, for their continued encouragement and support throughout the course of this study.

TABLE OF CONTENTS

LIST OF TABLES

LIST OF FIGURES

LIST OF SYMBOLS AND ABBREVIATIONS

E	Effective Dose
H_E	Effective Dose Equivalent
H(d)*	Ambient Dose Equivalent at depth d in the ICRU sphere
H'(d)	Directional Dose Equivalent at depth d in the ICRU sphere
H_p *(d)*	Individual Dose equivalent, penetrating
H_s*(d)*	Individual Dose equivalent, superficial
H_T	Organ Tissue Dose Equivalent
GEM	Gas Electron Multiplier
ICRP	International Commission on Radiation Protection
ICRU	International Commission on Radiation Units and Measurements
LET	Linear Energy Transfer
Q	Quality Factor
R	Roentgen
Sv	Sievert
TE	Tissue Equivalent
TEPC	Tissue Equivalent Proportional Counter
w_R	Radiation Weighting Factor
w_T	Tissue Weighting Factor

SUMMARY

The effective dose equivalent, H_E (or the effective dose, E) to an individual is the primary limiting quantity in radiation protection. However, techniques for measuring H_E for neutrons have not been fully developed. In this regard a new tissue equivalent proportional counter (TEPC) based on a gas electron multiplier (GEM) for measuring $H^*(10)$, which is a conservative estimate of H_E, for neutrons was designed and constructed.

The deposited energy distribution for two different neutron sources (a ^{252}Cf source and a AmBe source) was measured using the new TEPC. The measurements were performed using two different proportional gases: P-10 gas and a propane-based tissue equivalent gas at various pressures. A computer simulation of the new TEPC, based on the Monte Carlo method, was performed in order to obtain the pulse height distributions for the two neutron sources. The simulated results and the measured results were compared. Results show that the experimental results agree with the computational results within 20% of accuracy for both ^{252}Cf and AmBe neutron sources.

A new model GEM-based TEPC was developed for use in obtaining $H^*(10)$. The value of $H^*(10)$ for the ^{252}Cf source and for the AmBe source using experimental measurements was obtained. These results are presented in this study. The study shows that the GEM-based TEPC can successfully estimate $H^*(10)$. With these results and some refinements, this GEM-based TEPC can directly be used as a neutron rem meter.

CHAPTER 1

INTRODUCTION

Monitoring of radiation exposure to a person is an important aspect of radiation protection. The primary limiting quantity in radiation protection to an individual is the effective dose equivalent, H_E [1]. In a recent ICRP recommendation [2], H_E was replaced with a similar quantity, the effective dose, E. However, H_E and E are inherently not measurable, because they require knowledge of dose equivalence for various organs in the individual [1,2]. For this reason, measurable operational quantities were introduced, whose values ensure that the primary limits are not exceeded [3]. As recommended by the International Commission on Radiation Units and Measurements (ICRU), the operational quantities for individual monitoring of external penetrating radiations (e.g. neutrons and gamma rays) is called the dose equivalent, $H^*(10)$, defined as the dose equivalent measured at the depth 10 of mm inside a tissue-equivalent phantom [4]. $H^*(10)$ is a conservative estimate of H_E and E. Several techniques have been developed to measure $H^*(10)$ for gamma rays. However, the measurement of $H^*(10)$ for neutrons has never been fully satisfactory [5].

Recently a new type of tissue equivalent proportional counter (TEPC) based on gas electron multiplier (GEM) was developed [6]. The GEM-based TEPC does not need a central wire as anode, and thus makes it possible to construct a high-efficiency (or sensitivity) TEPC, ideal for measuring $H^*(10)$ for low levels of neutrons. The present research is motivated by such a possibility.

The objectives of the present study are: (1) to build the new GEM-based TEPC, and (2) to test its performance for measuring $H^*(10)$ for neutrons of two distinctly different energy spectra. This detector will be capable of making direct estimates of the $H^*(10)$ from a given set of measurements in any poorly-defined neutron field.

This thesis is organized as follows. Chapter 2 presents the background information on radiation protection dosimetry and the traditional measurement methods. A description of the GEM-based TEPC is presented in Chapter 3. Chapter 4 discusses the computational methods and results of the GEM-based TEPC for various neutron

measurements. Chapter 5 discusses the experimental design and procedure performed to test the GEM-based TEPC. Chapter 6 presents the results of the experimental studies and compares them with the computational results. Additional discussion is presented in chapter 7. Chapter 8 presents the conclusion of this study and recommendations for future work.

CHAPTER 2

BACKGROUND

2.1 Dose Quantities for Radiation Protection Dosimetry

Monitoring radiation exposure to an individual is an important aspect of radiation protection. It has been shown that high-level exposures to radiation result in varying degrees of harmful effects to the human body. At radiation exposures higher than 10 Gy, certain severe effects are observed within a few hours after exposure. [7] At intermediate levels radiation causes genetic effects in the offspring and carcinogenic effects to the exposed person. At very low levels of radiation exposure (lower than the average annual exposure to background radiation of 3.6 mSv), radiation effects are too small to be observed.

As it was stated by the International Atomic Agency (IAEA) in 1965 [8,9], the main purpose of monitoring the radiation exposure of individuals was to prevent over - exposure and to avoid the unnecessary exposure of personnel working with various sources of radiation. In 1980, this objective was rephrased in the revision of this IAEA document to be consistent with the International Commission on Radiological Protection (ICRP) recommendations. The main purpose of monitoring radiation exposure is now to keep it as low as reasonably achievable (the ALARA concept) and to make sure that limits are not exceeded. [9-11] Monitoring systems serve the following functions:

1. to give early indication of significant individual exposures;
2. to give prompt notice of accidental over-exposures;
3. to evaluate the radiation safety of working areas;
4. to observe trends of exposure histories of individuals or groups of workers;
5. to provide a record of information which may be needed for legal purposes

In 1977, ICRP published the recommendation to be used in measuring of the effect of radiation on an individual. This is the first formal and clear guideline on conducting radiation protection. This report introduced primary limiting quantities that were not inherently measurable by radiation monitors and equipment, simply because they are defined in the individual. Therefore it was necessary to introduce operational

quantities that are conservative estimations and can be related to the primary limiting quantities. In 1985 the International Commission on Radiation Units and Measurements (ICRU) introduced the operational quantities.

The quantities presented below are to avoid confusion in the terminology of quantities used in radiation protection. The first group of quantities is the primary limiting quantities recommended by the ICRP. The second group of quantities is the operational quantities that are amenable to measurements using field instruments and personnel dosimeters with standard phantoms and irradiation geometries. These quantities are usually presented by ICRU.

2.1.1 The Primary Limiting Quantity

In the 1977 Report 26 of the ICRP [12], the primary limiting quantity is introduced as a means of estimating the risks to the workers in the radiation industry. The reason for introducing limits to the primary quantities is to prevent harmful non-stochastic effects in any single organ of an individual and to keep the total stochastic risks for the radiation workers below an acceptable standard. Before the ICRP-26 recommendations, a single limit of 0.2 R/day was applied for the whole body of an individual. In 1951, ICRP defined limits for low penetrating radiation such as β particles - 1.5 R/week and electrons and high penetrating radiation like X-rays and γ rays - 0.05 R/week. Limits for different organs of the body were introduced, as more information about the biological effects of radiation became available. [13] Guidelines for radiation protection introduced in the ICRP 9 report considered the whole body dose equivalent and the concept of the critical organ. The whole body dose equivalent limit was set at 50 mSv/year and critical organs have their own specific limits. After ICRP-26 weighting factors are assigned to each organ proportional to their known radiosensitivity and risk factors. The whole body dose equivalent limit remained at 50 mSv/year. ICRP introduced the primary limiting quantity in 1977. The quantity is called the effective dose equivalent, H_E. It is defined as the following:

$$H_E = \sum_T \omega_T \times H_T \qquad (2.1)$$

where w_T is called the tissue or organ weighting factor and H_T is the tissue or organ dose equivalent. H_T is defined as

$$H_T = \sum_i D_{T,i} \times \overline{Q}_i \qquad (2.2)$$

where $D_{T,i}$ is the mean absorbed dose in the organ or tissue T from the incident radiation of type i, $\overline{Q}_i$ is the corresponding effective quality factor for the incident radiation of type i . $\overline{Q}_i$ is defined as a function of the collisional stopping power (L_∞) , or linear energy transfer, LET [14]. For neutrons,. $\overline{Q}_i$ is the effective quality factor at the point of interest depends on the spectrum of secondary charged particles at given point. $\overline{Q}_i$ is 1 for γ rays. The direct way of applying H_E would be to measure the organ dose equivalents in routine monitoring and applying the appropriate tissue weighting factors. But this is not possible, because there is no correct way of directly measuring the organ dose equivalent of a person. Therefore the operational quantities were introduced as a way of providing a conservative estimate of the primary limiting quantity.

The ICRP also introduced the secondary limits for external exposure in their 1977 recommendations. Secondary limits are defined as: "In the case of external radiation of the whole body, the secondary limit applies to the maximum dose equivalent in the body at depths below 1 cm". Furthermore, "When information is lacking concerning the actual distribution of dose equivalent in the body, it is possible to assess the maximum value of dose equivalent that would occur in 30 cm sphere (the deep dose equivalent index, H_I)" This means that the operational quantity H_I could be taken to represent the secondary limiting quantity.

In 1990, the ICRP [15] published new recommendations relating to quantities and dose limits in radiation protection. The new recommendations significantly differ from those given in ICRP-26. Among the new recommendations of the ICRP Report 60, the following changes have significant implications:

1. The primary limiting quantity is now called effective dose, E, defined as the sum of the weighed equivalent doses in all the tissues and organs of the body, i.e.

$$E = \sum_T \omega_T \times H_T \qquad (2.3)$$

where H_T is now called the equivalent dose in the tissue, T, and w_T is the tissue weighting factor.

2. The average dose equivalent in tissue, T, defined in ICRP-26 is now replaced with the equivalent dose, H_T , defined as

$$H_T = \sum_R \omega_R \times D_{T,R} \qquad (2.4)$$

where $D_{T,R}$ is the mean absorbed dose in the tissue or organ - T due to radiation - R and w_R is the radiation weighting factor. w_R replaces the effective quality factor, Q and w_R is based on the incident spectrum. This is used to relate the relative degree of detriment to the tissues from the incident radiation. A new set of w_T values were introduced where more organs have explicit values and the remainder is defined differently. These new values remove the need for limits on specific organs or tissues except for the lens of the eye, skin and extremities. Table 2.1 shows the ICRP-26 and ICRP-60 w_T values for the different organs in the body. Organs defined in the remainder have also changed.

3. New dose limits were recommended. An effective dose limit of 100 mSv over a 5 year period with a maximum of 50 mSv in any single year for occupationally exposed persons.

Table 2.1: Comparison of the w_T values from ICRP-26 and ICRP-60. * Remainder in ICRP-26 refers to the rest of the 5 of the organs receiving the highest dose equivalents which are assigned a w_T value of 0.006. ** Remainder in ICRP-60 is distributed in the following 10 organs: adrenals, brain, ULI, SI, kidney, muscle, pancreas, spleen, thymus and uterus.

Organ	ICRP-26 w_T	ICRP-60 w_T
Gonads	0.25	0.2
Breast	0.15	0.05
RMB	0.12	0.12
Lungs	0.12	0.12
Bone Surface	0.3	0.01
Thyroid	0.3	0.05
Colon	-	0.12
Stomach	-	0.12
Liver	-	0.05
Esophagus	-	0.05
Bladder	-	0.05
Skin	-	0.01
Remainder	0.3*	0.05**

2.1.2 The Operational Quantity

It is not possible to directly apply the primary limiting quantities to routine monitoring because they are defined in the individual. Therefore it was necessary to introduce operational quantities whose limitations ensure that the primary limits are not exceeded.

According to ICRU, the operational quantities for area monitoring are the ambient dose equivalent, $H^*(d)$, and directional dose equivalent, $H'(d)$, and those for individual monitoring are the individual dose equivalent, penetrating, $H_p(d)$, and individual dose equivalent, superficial, $H_s(d)$. The definitions of the operational quantities are provided below.

1. The ambient dose equivalent, $H^*(d)$ is defined as the dose equivalent at a point of a radiation field that would be produced by the corresponding aligned and expanded field, in the ICRU sphere(i.e. a 30-cm-diameter sphere made of a tissue-equivalent material) at a depth d, on the radius opposing the direction of the aligned field.
2. The directional dose equivalent, $H'(d)$ is defined as the dose equivalent at a point in a radiation field that would be produced by the corresponding expanded field in the ICRU sphere at a depth, d , on a radius in specified direction.
3. The individual dose equivalent, penetrating, $H_p(d)$ is defined as the dose equivalent is soft tissue, below a specified point on the body at a depth, d, that is appropriate for strongly penetrating radiation.
4. The individual dose equivalent, superficial, $H_s(d)$ is defined as the dose equivalent in soft tissue below a specified point on the body at a depth, d, that is appropriate for weakly penetrating radiation.

The recommended depth in the ICRU sphere phantom for $H^*(d)$ and $H_p(d)$ is 10 mm while the recommended depth for the $H'(d)$ and $H_s(d)$ is 0.07 mm. [16]

This study focuses on the measurement of $H^*(10)$, i.e. $H^*(d)$ where d=10 mm for neutrons.

Several calculations of the $H^*(10)$, are available . [17-22]

Fig. 2.1 presents the fundamental curve $H^*(10)/\Phi$, where Φ is neuron fluence. [23]

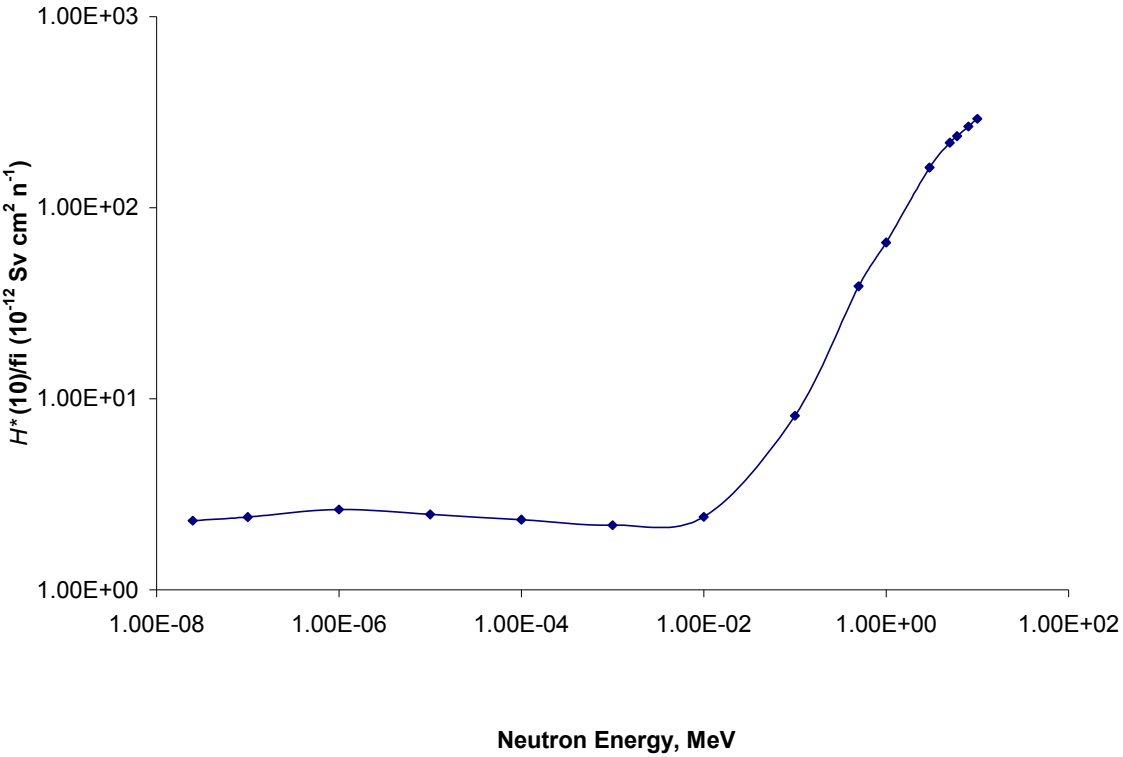

Figure 2.1 Ambient dose equivalent $H^*(10)$ per unit fluence. [23]

2.2 Traditional Measurement Methods

Traditional methods for real-time neutron dose monitoring can be classified into three categories. The first category is based on placing a thermal neutron detector (e.g. a $^{10}BF_3$ proportional counter or a ^{6}LiI scintillation detector) inside a large polyethylene sphere (or cylinder). Incident neutrons are moderated in the polyethylene and then detected by the thermal neutron detector. It was noted that, if one uses a 10 inch diameter sphere of polyethylene, then there is a close fit between the detector's efficiency and the effective dose equivalent, H_E, per incident neutron over a wide range of neutron energy [23]. In other words, the count rate is directly proportional to H_E regardless of the energy spectrum of the incident neutron. The major disadvantage of such a system, however, is that the large thickness of the polyethylene sphere necessarily makes it too heavy to be carried by an individual. Nevertheless, such systems remain the most widely used ones in industry today.

The second category is often referred to as either the superheated liquid drop detector (SLDD) or the bubble damage detector (BDD) [24,25]. The active volume of these detectors is based on a suspension of many small liquid freon droplets held within a gel or polymer matrix. Under regular conditions of temperature and pressure, the droplets of freon are in a metastable (or superheated) state. They are ready to flash into a vapor, but a trigger is required. That trigger can be provided by the recoil nuclei (or ions) produced by incident neutrons. It has been shown that the number of vapor bubbles is a measure of H_E for neutrons with energies above 100 keV. The advantages of these detectors are: (1) they have very high sensitivities for detecting neutrons, and (2) they are totally insensitive to gamma rays. However, they also have several obvious drawbacks: (1) they are susceptible to temperature change of the environment, (2) they often produce large errors in the measurements of H_E due to the 100-keV neutron threshold, and (3) they are not reusable after the droplets have been depleted.

The third category uses a tissue-equivalent proportional counter (TEPC) to measure the energy deposition distribution, $f(\varepsilon)$, of the recoil nuclei (mainly protons). This category is the least popular one. The energy deposition distribution is then converted to the lineal-energy distribution $f(y)$ via the following relationship:

$$y = \frac{\varepsilon}{\bar{l}} \tag{2.8}$$

where $\bar{l}$ is the mean chord length of the tissue target represented by the TEPC's gas cavity. The distribution $f(\varepsilon)$ can be used to obtain the absorbed dose D, which is then combined with the distribution $f(y)$ to obtain the dose equivalent H via a ICRU-recommended radiation quality factor function $Q(y)$. [26] Specifically, the ICRU-recommended function $Q(y)$ corresponds to a $\bar{l}$ value of 1 μm, which is usually represented by a 0.5 inch-diameter TEPC operated at 0.1 atm of gas pressure. Because of its small size (and therefore low detection efficiency), such a TEPC suffers from low sensitivities in neutron detection. [27] To improve the sensitivity by increasing the cavity size, however, would make the value of $\bar{l}$ exceed the ICRU-recommended 1 μm, which invalidates the use of the ICRU-recommended function $Q(y)$. These arguments necessarily explain why TEPCs have not been commonly used in neutron protection dosimetry.

The recent invention of gas electron multiplier (GEM), however may change the trend because the GEM allows one to construct a plate-like TEPC so that many of the GEM-based TEPCs can be stacked together in a single device to dramatically increase its neutron sensitivity. [28] This study focuses on the construction and test of a GEM-based TEPC for measuring $H^*(10)$ for neutrons.

CHAPTER 3

GEM-BASED TEPC

3.1. Characteristics of GEM

The gas electron multiplier (GEM) was first developed by F. Sauli at CERN, European Organization for Nuclear Research [29]. It is a copper coated Kapton foil (on both sides), perforated with a high density of holes (typically 50 to 100 per mm^2). Etched in a photolithographic process, these holes have diameters of about 70 μm. The holes are spaced with a pitch of usually 140 μm (standard geometry), [30] as shown in Fig. 3.1. Application of a potential difference between upper and lower copper layer creates a high electric field inside the holes as Fig. 3.2 illustrates. By properly applying the electric potentials, electrons produced in the upstream of the GEM can be guided into these holes, where they undergo gas amplification. [30] The multiplication of the electrons results in effective gains well above 10^2. The total effective gain obtained with such a detector can be adapted to the needs of the application by choosing the proper voltage across the GEM. The major advantage of the GEM detector is the separation of gas amplification and readout stage. This separation results in a fast readout-signal (because only electrons are collected by the readout structure).

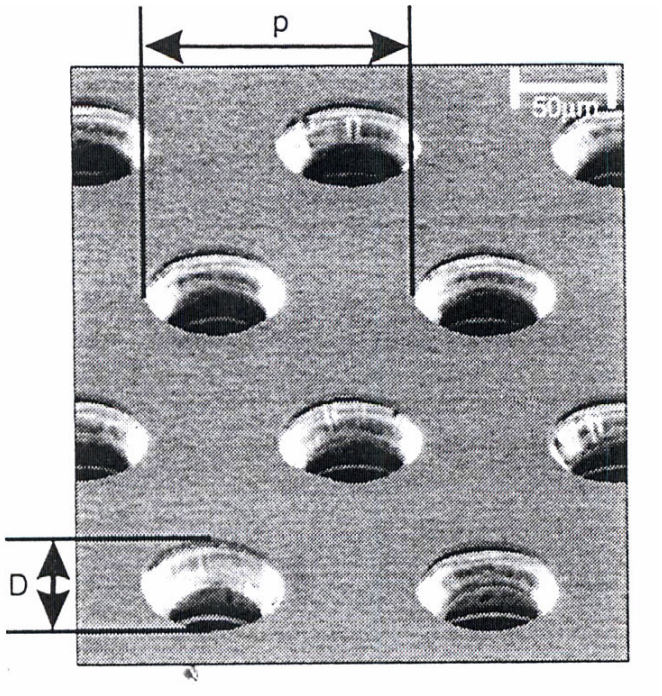

Figure 3.1. The electron microscope photograph of a GEM foil with standard geometry. The pitch p=140μm, and the outer hole diameter D=70 μm. [30].

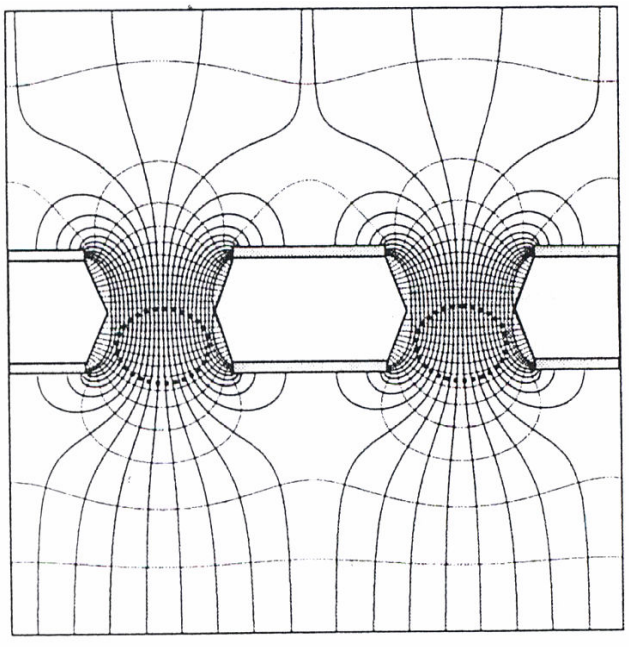

Figure 3.2. Electric field lines in a GEM foil.[30]

A GEM can be used as a single GEM detector or by cascading several GEMs in a single device [30-31]. The latter configuration allows large overall gains to be reached in a radiation environment. In addition, there are advantages of the signal formation by electron collection in the GEM. It leads to faster signal collection in contrast to positive ion collection in many other systems. The efficiency will affect the pulse height resolution in applications where a relatively large number of primary electrons are released within the gas volume preceding the GEM, e.g. microdosimetric measurements. The electron collection efficiency is a crucial issue, particularly for single photons or electrons detection. It depends on the given GEM geometry, the electric field above and across the GEM, and the gas type composition and pressure.

In addition to electron collection efficiency, there are more considerations to ensure optimal GEM operation. In particular, a substantial fraction of avalanche electrons may be drawn to the bottom of the GEM electrode instead of the collection plane. Those electrons will not contribute to the readout signal. That will result in a lower effective GEM gain. This can be optimized by proper choice of the electric field configuration and geometry.

3.2 Design Configuration of the GEM-Based TEPC

The schematic of the design of the new GEM-based TEPC for measuring $H^*(10)$ for neutrons is shown in Fig. 3.3. The 3-D exploded view of the same GEM-based TEPC is presented in Fig 3.4. The system consists of mainly four layers of materials – A-150 conducting plastic (as the cathode), the GEM foil and the copper layer (as the anode). The polyethylene slab is 1 cm thick, and it was designed to match the thickness of 10 mm specified for H^* (10). The A-150 layer is 2-mm thick. The GEM has an active area of 5 cm × 5 cm. Two Rexolite guard frames were used as the insulator to separate the GEM foil from A-150 and copper. The region between A-150 and GEM is the gas cavity (i.e. the charge drift region), which is 4-mm thick and filled with a proportional gas. The region below the GEM is the charge collection region, which has a thickness of 2 mm and a gas content the same as that of the charge drift region. The A-150 layer, acting as the cathode, will be held at the ground potential and the anode will be held at the positive voltage during the operation. As indicated in Fig. 3.3 the total voltage across the system is divided by three resistors 10 MOhm, 50 MOhm and 10 MOhm. These resistors divide

the total voltage with the proportion 1:5:1. For example, if a total voltage of 700 volts is applied to the system than 100 volts will be applied between A-150 and the top side of GEM, 500 volts will be applied between the top side and the bottom side of GEM, and 100 volts will be applied between the bottom side of GEM and the copper anode.

Also shown in Fig. 3.3, the incident neutrons interact in the layer of A-150 and produce energetic charged particles (i.e. protons). The protons, in turn, may enter the gas region and create ionization events (i.e. electrons and ions). The electrons produced in the gas region will drift into the holes of GEM, get multiplied, and then collected by the copper anode.

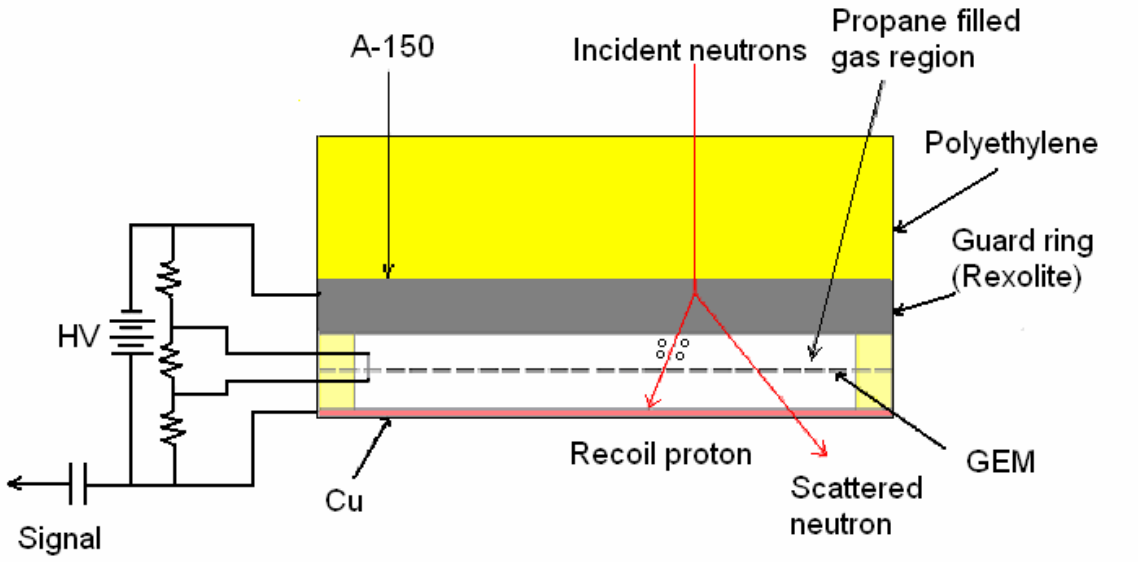

Figure 3.3. A single-layer GEM-based TEPC.

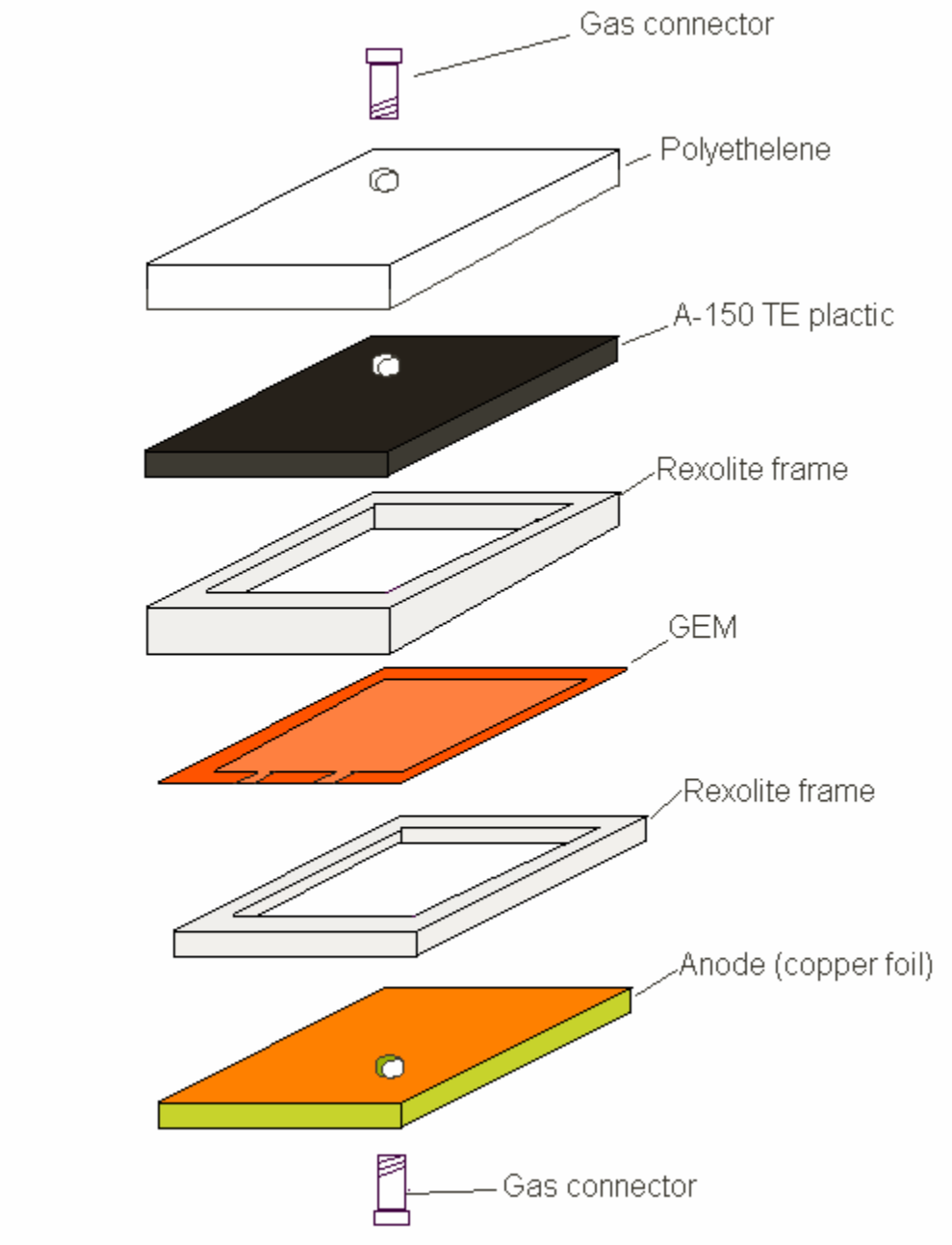

Figure 3.4. Exploded view of the GEM-TEPC.

3.3 Construction of the GEM-based TEPC

Assembly of the GEM-based TEPC is entirely carried out in the cleanroom of the School of Electrical and Computer Engineering at the Georgia Institute of Technology. A cleanroom environment is necessary because dust particles may lodge in the GEM holes and cause catastrophic electrical discharges during operation. A custom-made, frame was used to assemble the detector. The different elements are cleaned and kept inside the clean room before assembly. After being assembled the detector was sealed with glue and then continuously flushed with clean nitrogen at an elevated temperature of 40 ^{o}C for 24 hours to avoid concentration of vapors and speed up the glue polymerization.

The high voltage (HV) test of the GEM was conducted at different stages during the assembly process. The leakage currents across the GEM foil were measured for various voltages. The purpose of the HV test was to ensure that leakage current does not exceed the limit of 5 nA, beyond which the GEM is not usable [32]. The test results are provided in Table 3.1, which show that the measured leakage currents are indeed much lower than 5 nA.

Table 3.1 Leakage current across the GEM

Voltage, V	Leakage current, A (before being assembled)	Leakage current, A (after being assembled)
50	6×10^{-11}	9×10^{-11}
100	7×10^{-11}	1.5×10^{-10}
150	9×10^{-11}	2.4×10^{-10}
200	9×10^{-11}	3.2×10^{-10}
250	10×10^{-11}	4.1×10^{-10}
300	7×10^{-11}	4.8×10^{-10}
350	10×10^{-11}	5.8×10^{-10}
400	7×10^{-11}	6.4×10^{-10}
450	1.2×10^{-10}	7.3×10^{-10}
500	2.1×10^{-10}	8.2×10^{-10}
550	2.4×10^{-10}	8.9×10^{-10}
600	2.5×10^{-10}	
650	2.6×10^{-10}	

3.3.1 Construction Procedure

1. Component Cleaning

The detector components (A-50 plastic, Rexolite frames, anode, polyethylene slab) were cleaned in an ultrasonic bath with deionized water for 5 minutes. The cleaning procedure is described below:

a) Place components into the cleaning-beaker, fill the beaker with deionized water and place the beaker into the ultrasonic bath for 5 minutes.

b) Place the components in the oven at 40 ^{o}C for 4 hours, until they are completely dry.

2. High Voltage Test for GEM

a) Gently flush the GEM foil with the nitrogen gun to remove dust.

b) Apply various voltages between 0 and 650 volts (in steps of 50 volts) HV to the GEM foil and measure the leakage currents across the GEM to make sure that the leakage currents are below the required limit of 5 nA.

3. Assembly of the components

a) Prepare the glue by mixing the hardener and resin together in the plastic container.

b) Assemble the top portion of the detector by applying the glue to the gas connector, polyethylene slab, A-150 plastic, rexolite frame as shown in Fig. 3.5.

c) Place the top portion of the detector into the oven at 40 ^{o}C for 24 hours.

d) Assemble the bottom portion of the detector by applying the glue to the rexolite frame, anode and gas connector as shown in Fig. 3.6.

e) Assemble top and bottom portions of the detector and place it into the oven at 40 ^{o}C for 24 hours.

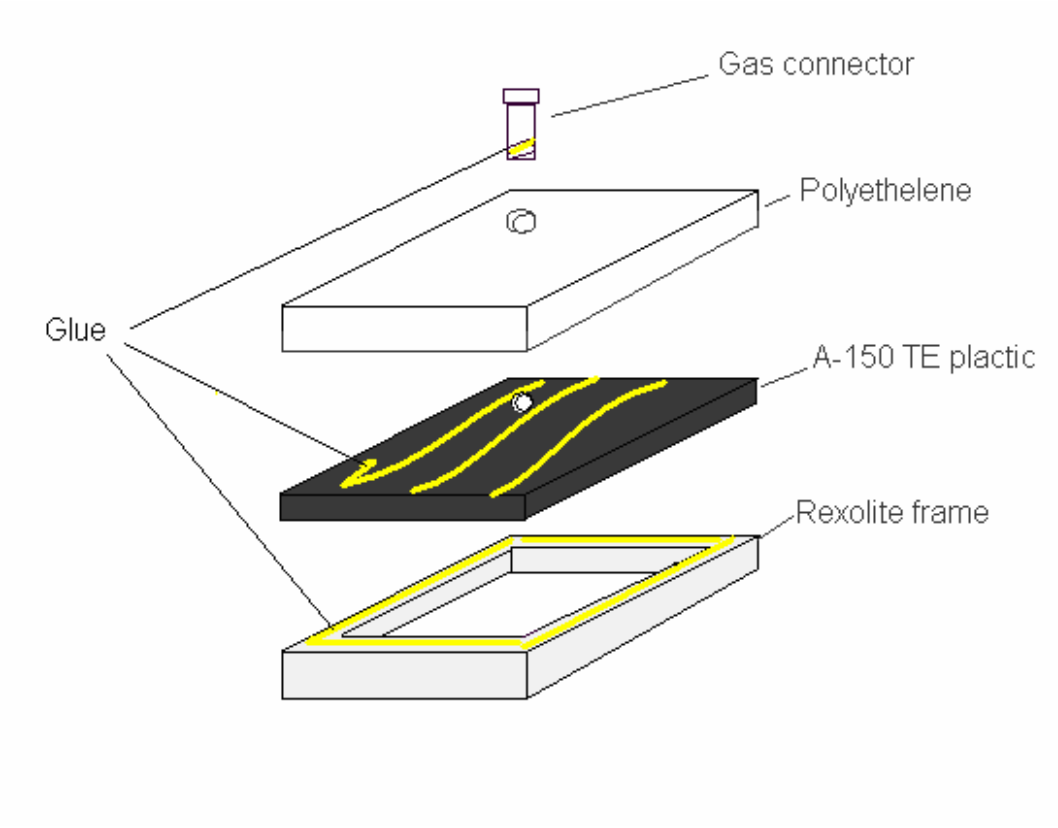

Figure 3.5. Assembly of the top portion of the detector.

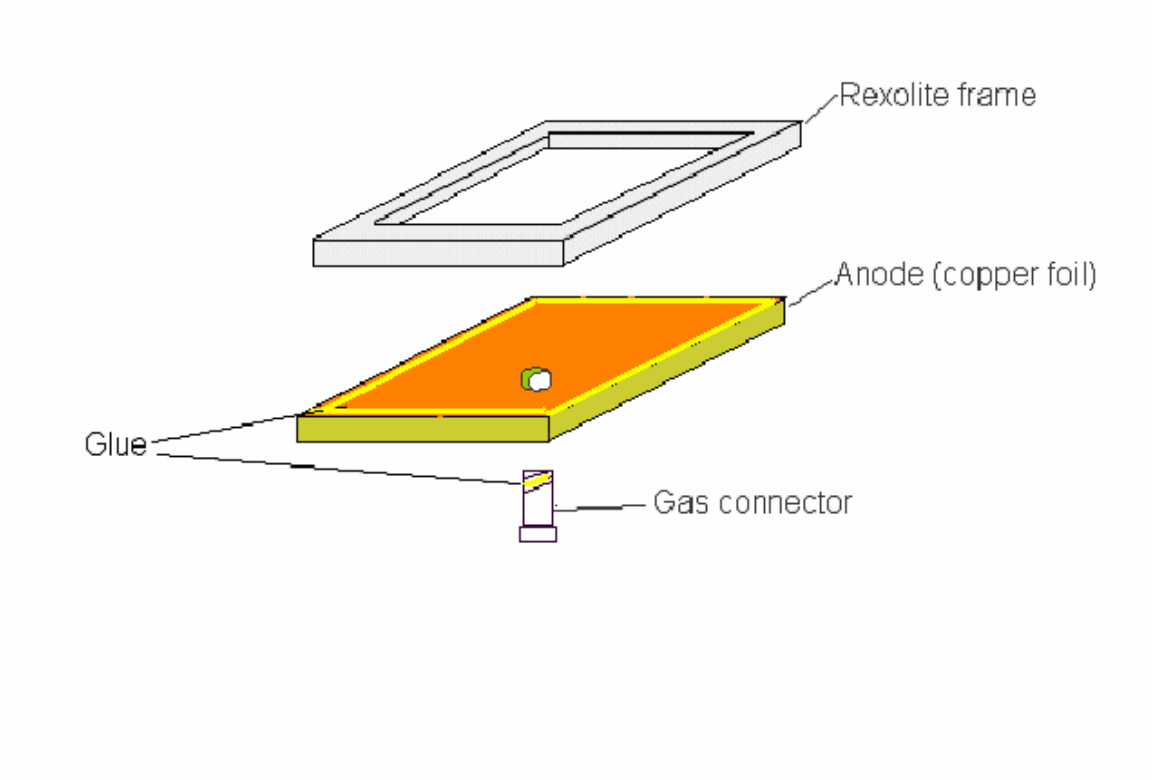

Figure 3.6. Assembly of the bottom portion of the detector.

4. Mounting GEM onto Rexolite frames.

Due to its floppiness, the GEM foil needs to be first fixed and stretched with a Plexiglas transfer frame (see Fig.3.7.), which was then glued to the detector assembly. The entire GEM mounting procedure is provided below.

a) Apply glue on the Kapton surrounding the copper-coated area of the GEM foil. (see Fig.3.7.)

b) Attach the two Rexolite frames to the top and bottom of the GEM foil.

c) Conduct HV test.

d). Put the assembley into the oven.

e) Connect the N_2 flow to the gas connectors and set the flow to 20 cc/min.

f) Dry the assembly for 24 hours under 40^o C.

g) Conduct the HV test again.

5. Putting everything together.

The various portions of the detector were then glued and sealed together, and the fully assembled detector is shown in Fig. 3.8. In order to reduce the electronic noise the detector must be placed into the metal box. The box will act as a shield for the electromagnetic waves in the environment. The box was made of thin aluminum sheet, and also contains the resistor circuit described in Fig.3.4. The final view of the detector is presented in Fig. 3.9. The connector on the top is for gas flow. The connector on the side is for signal/HV, and is can be directly connected to a preamplifier such as the ORTEC 142PC.

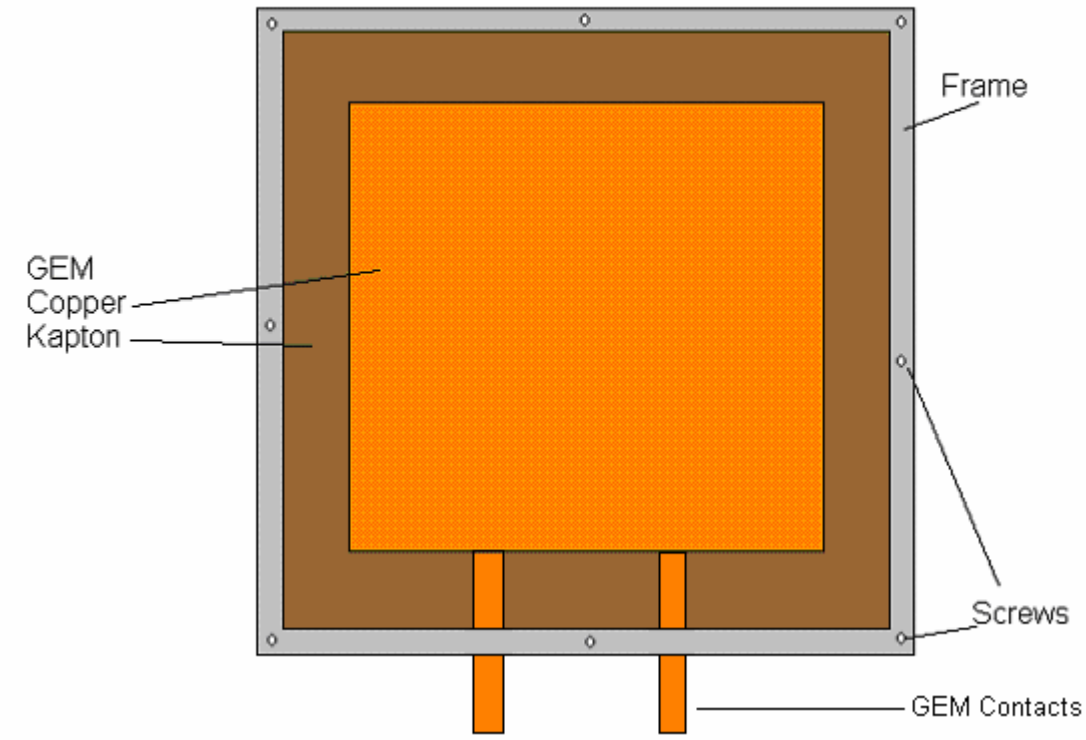

Figure 3.7. GEM foil was fixed on a Plexiglas transfer frame before it was glued to the Rexolite frames.

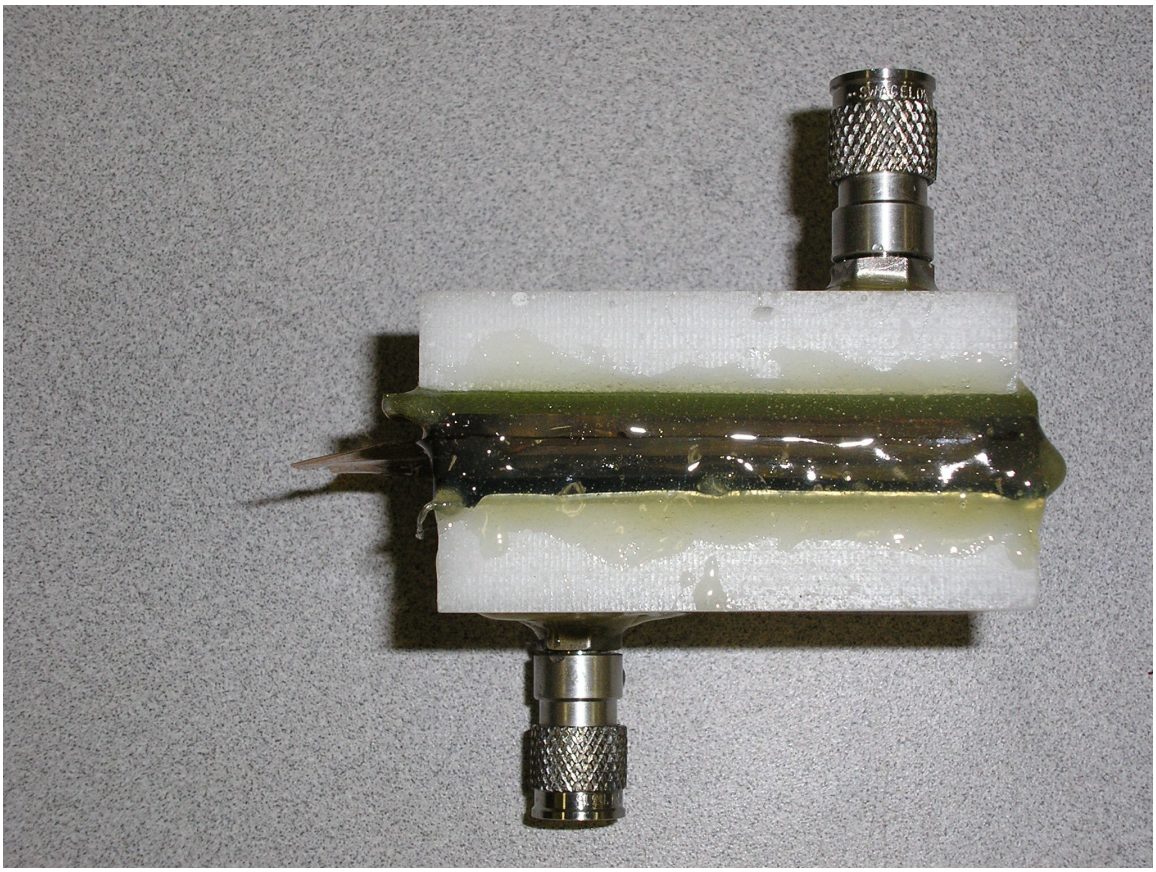

Figure 3.8. The fully assembled detector.

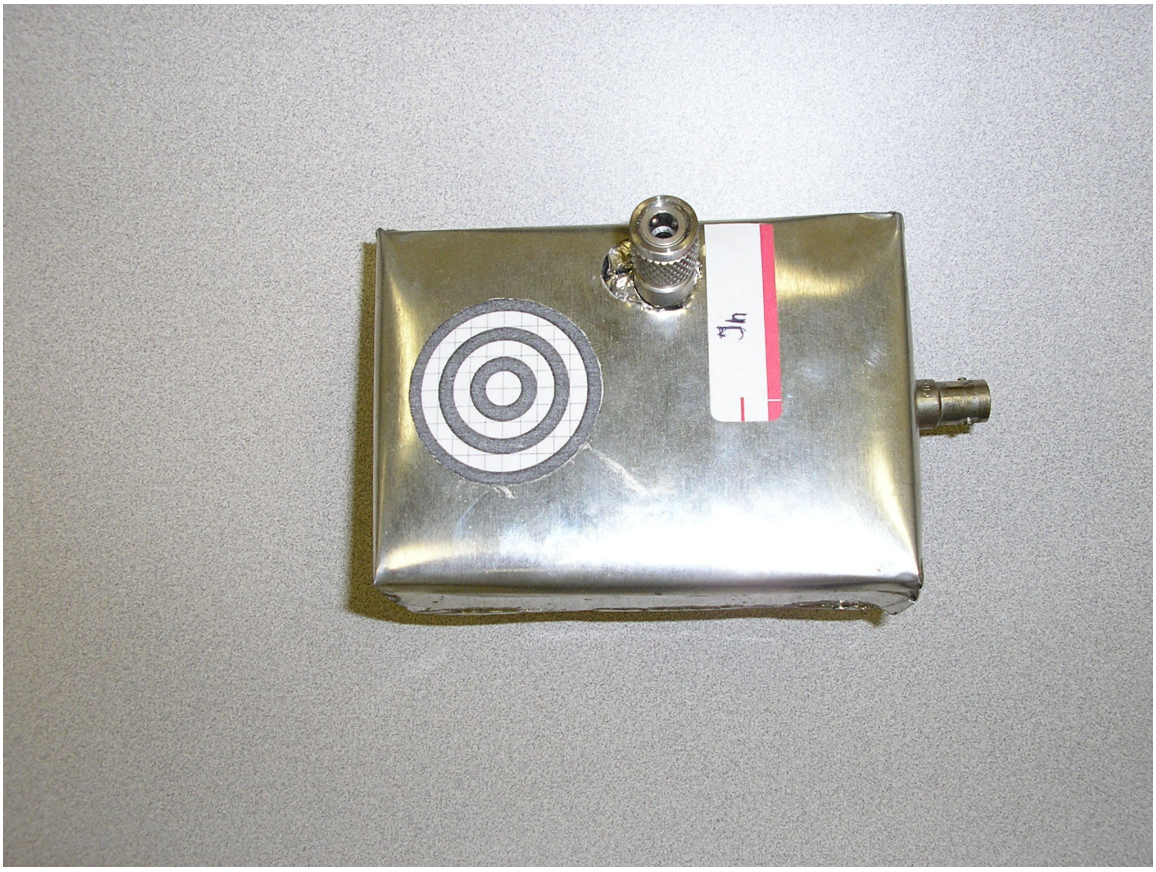

Figure 3.9. Final view of the GEM-based TEPC.

CHAPTER 4

COMPUTATIONAL STUDY

Since the GEM-based TEPC is to be used to measure the pulse height distribution (PHD) of the neutron and gamma-ray events, a computational study on the detector's PHD response to neutrons and gamma rays has been performed. The main purpose was to produce a set of computational results that can be used to verify the detector's response obtained from the experimental measurements. Another purpose was to determine the GEM-based TEPC's ability to obtain the ambient dose equivalent ($H^*(10)$) for neutrons.

4.1 Simulation Method

A FORTRAN program was written based on the Monte Carlo method to simulate the response of the GEM-based TEPC to neutrons and gamma rays. The geometric configuration of the simulation is described in Fig.4.1 using an incident neutron as the example. In this case, the incident neutron undergoes an elastic scattering with a hydrogen nucleus in A-150, and the recoil proton enters the gas region (propane) and deposits some energy in the gas region. The contribution from the $^{14}N(n,p)^{14}C$ reaction in A150 is negligible, and therefore ignored in the simulation. The FORTRAN program follows histories of a large number of incident particles (neutrons or gamma photons) and tallies the energy depositions in the gas region. The detector's response, in this case, is defined as the energy deposition distribution (or histogram) normalized to one incident particle, i.e. per neutron or gamma photon. The flow chart of the program is provided in Fig. 4.2. The program statements are provided in Appendix A. The flow of the program is further described by the following procedure.

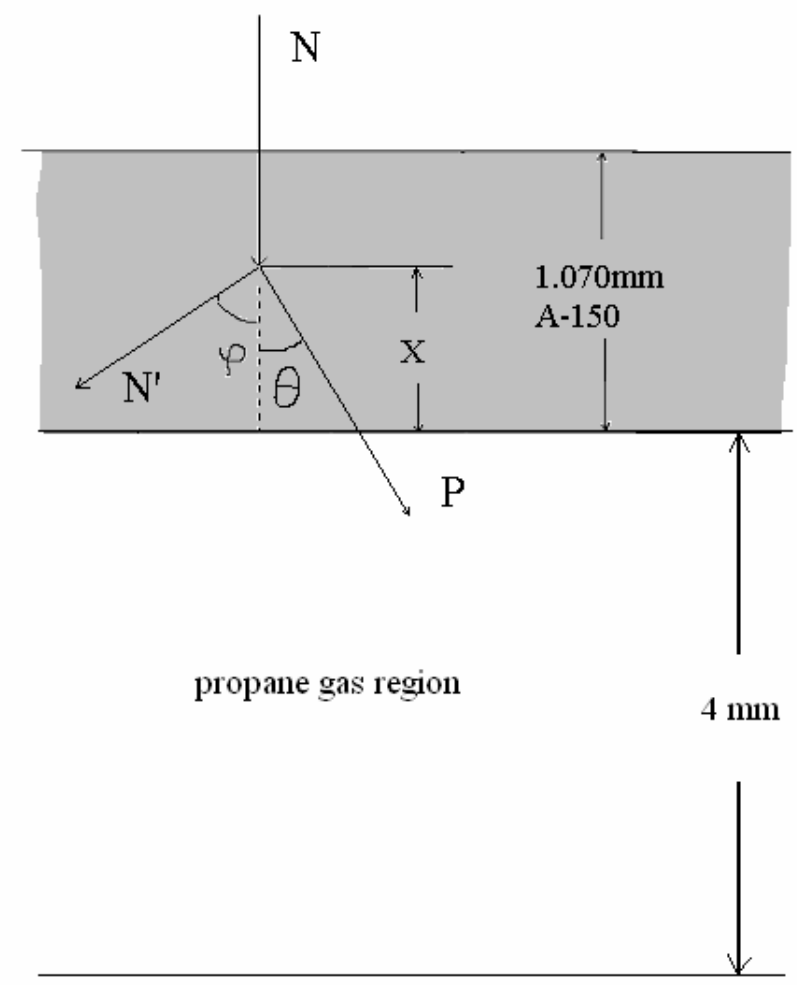

Figure 4.1. An interaction in A-150 (N is the incoming neutron, N' is the neutron after it makes an interaction, P is the recoil proton, X is the starting position of P, θ is the angle of P, and φ is the angle of N').

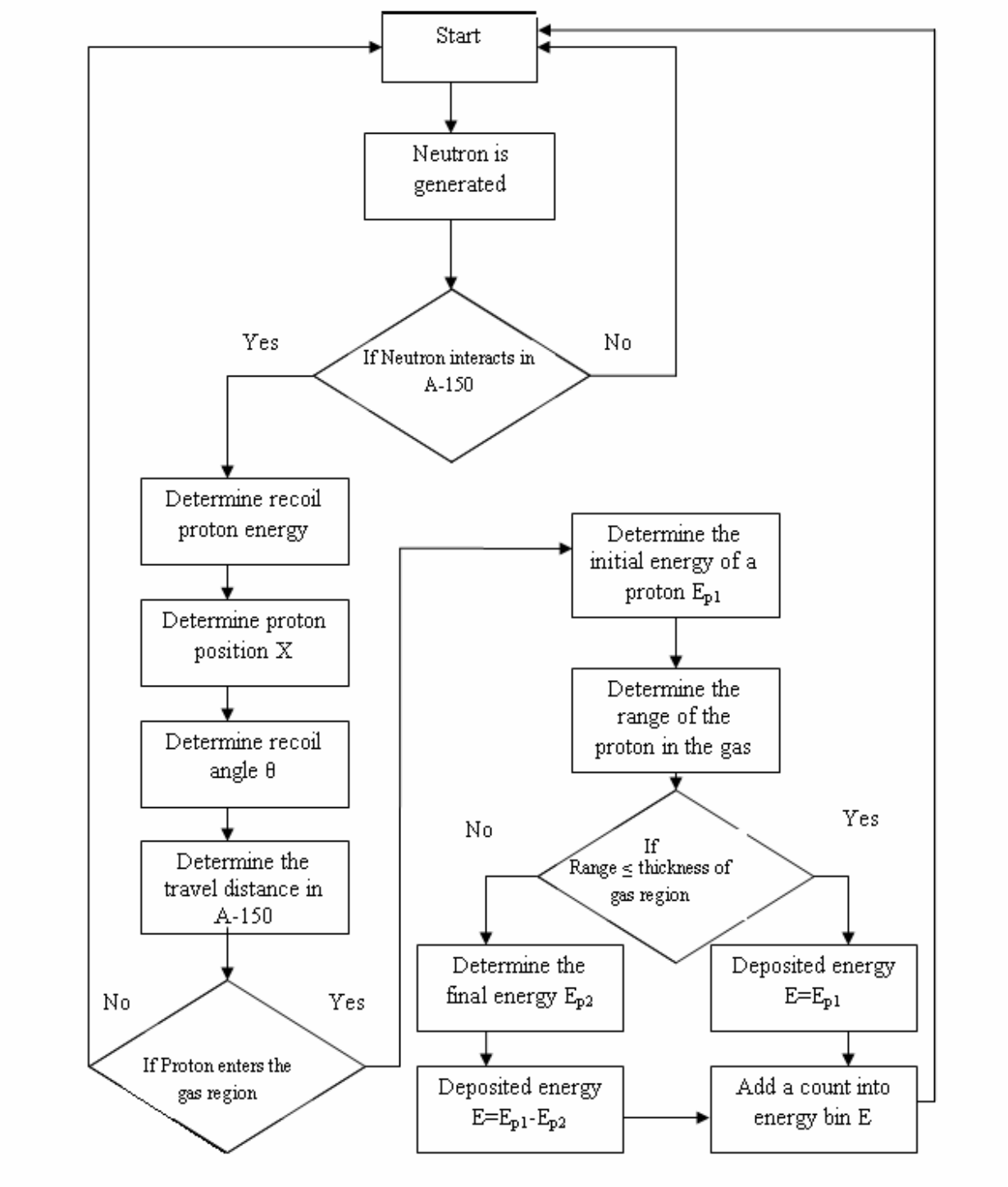

Figure 4.2. Flow chart of the FORTRAN program (see Appendix A) that simulates the response of the GEM-based TEPC to neutrons and gamma rays

1. The first neutron is processed.
2. Whether or not the neutron interacts in A-150 plastic is determined. If it does not interact, the next steps in the program are not carried out, and another neutron is processed. If it does interact, the program moves on to the next step.
3. The proton energy is determined.
4. The starting position X of the proton is selected. Refer to Fig.4.1.
5. cosθ, is determined using the relationship

   $$E_p = \cos^2\theta \cdot E_n \qquad (4.1)$$

   E_p and E_n are energies of proton and incident neutron respectively
6. The distance that proton travels in the A-150, is determined.
7. If that travel distance is not enough for the proton to enter the propane, a new neutron is processed. If the distance is long enough it goes to the next step.
8. The energy of the proton when it enters the propane is determined.
9. Determine if the proton is a stopper or crosser.
10. If the proton is a stopper, which means it stops in the gas, the energy deposited into the gas is equal to the energy of the proton before entering the gas region.
11. If the proton is a crosser, which means it penetrates to the other side of the GEM, then the energy that it has before passing the GEM, is determined. The energy deposited in the propane is then

    $$E = E_{p1} - E_{p2} \qquad (4.2)$$

    Where E_{p1} and E_{p2} are initial and final (before passing the GEM) energies of the proton respectively
12. The spectrum is created by placing a count into the bin corresponding to the energy deposited by the proton.

4.2 Simulation Results

4.2.1 Response to Monoenergetic Neutrons

Figure 4.3 shows the simulated results of the detector's response to neutrons of various energies. As indicated, the response is represented as the energy deposition distribution normalized to one incident neutron. It shows that low-energy neutrons deposit more energy in the gas than the high-energy neutrons and that the detection efficiency (i.e. counts n^{-1}) increases as neutron energy increases. The former can be explained by the LET effect. That is, LET of a proton increases as the proton energy decreases, and therefore, the recoil protons produced by neutrons of low energies (i.e. 0.5 MeV and 1 MeV) tend to deposit more energy. The latter can be explained by the proton – range effect. That is, the energetic recoil protons produced in A-150 by high-energy neutrons tend to have longer ranges than those produced by low-energy neutrons, and therefore, have higher probability of reaching the gas region.

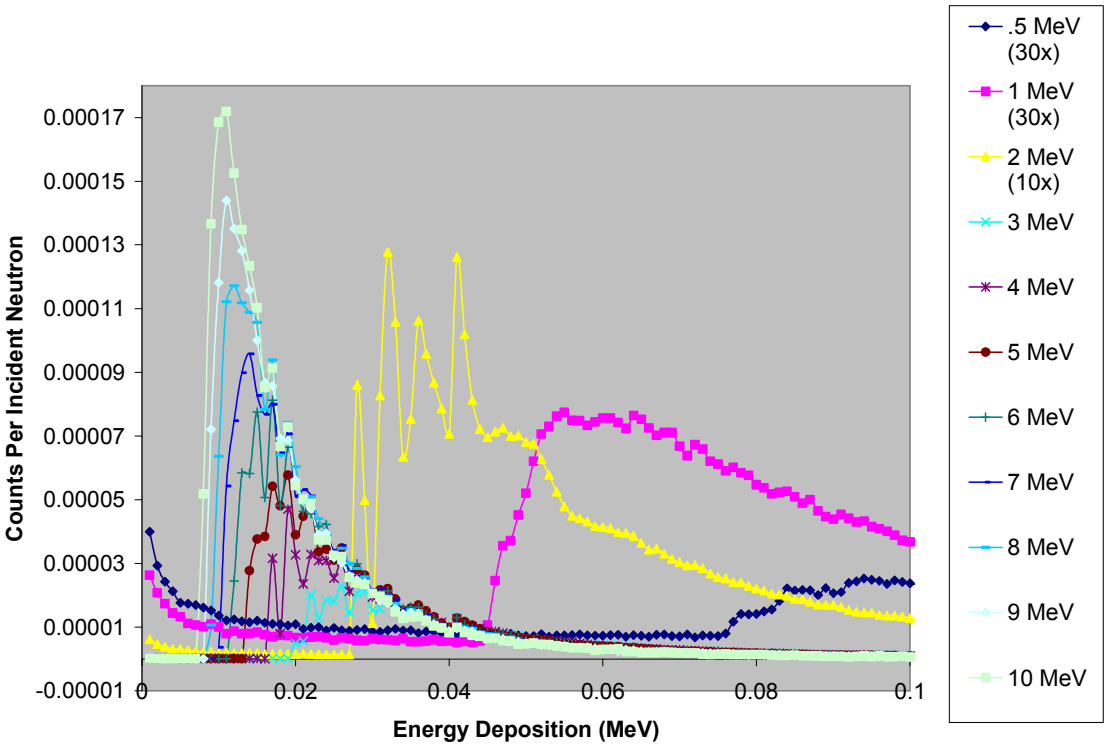

Figure 4.3. The simulated results of the detector's response to neutrons of various energies.

4.2.2 Response to ^{252}Cf and AmBe Neutrons

Two neutron sources (^{252}Cf and AmBe) were used in the experiments of this study (see chapter 5). These two neutron sources have very different energy spectra. As shown in figures 4.4 and 4.5, the most probable neutron energies occur at 0.85 MeV and 5 MeV for ^{252}Cf and AmBe, respectively [33,34]. To obtain the detector's response to the two neutron sources, one simply multiplies the monoenergetic neutron response curves (i.e. Fig. 4.3) with the corresponding probabilities (i.e. Fig.4.4 and Fig. 4.5.) and then adds them together. Figures 4.6 and 4.7 show the results for ^{252}Cf and AmBe, respectively. As shown for both cases, most neutron events have energy depositions les than 0.05 MeV. The few events that exceed 0.05 MeV are attributed to the protons that have very long tracks in the gas region – i.e. those who enter the gas region in the direction nearly parallel to the detector's plane.

One can also see by comparing Figures 4.6 and 4.7 that the count rate for AmBe neutrons is higher than the count rate for the ^{252}Cf neutrons and that the energy depositions are lower for the AmBe neutrons than that for the ^{252}Cf neutrons. The above observations are consistent with the fact that the Am-Be neutrons are on average more energetic that the ^{252}Cf neutrons.

The oscillations of the detector's response shown in Figures 4.3, 4.6 and 4.7 are somewhat unexpected, and the reasons for there oscillations are unknown. One possible explanation is from the fact that the energy and direction of the scattered proton are correlated (see equation 4.1).

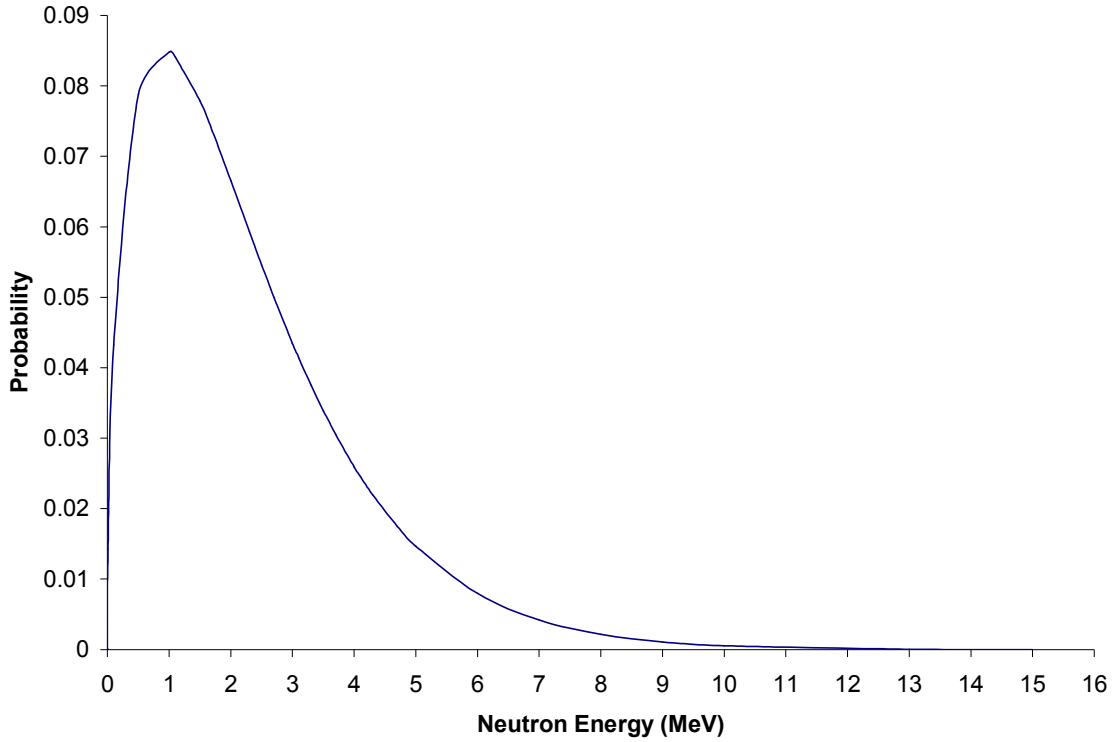

Figure 4.4. Energy spectrum of Cf-252 neutrons.

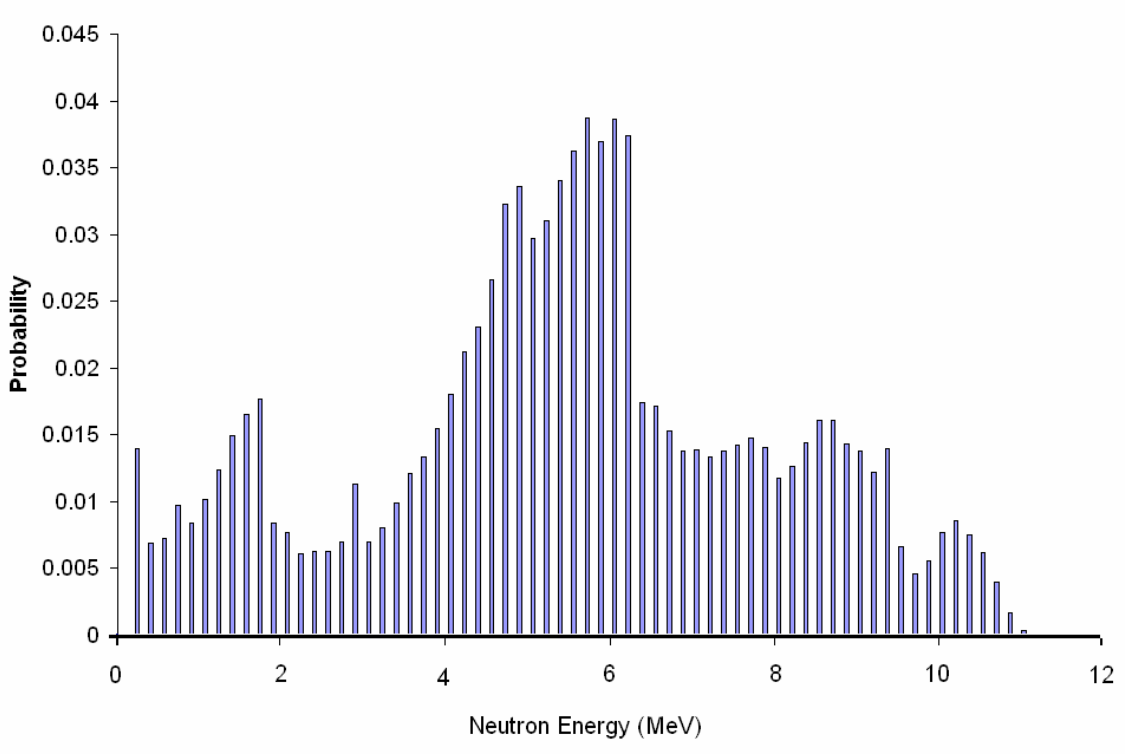

Figure 4.5. Energy spectrum of AmBe neutrons.

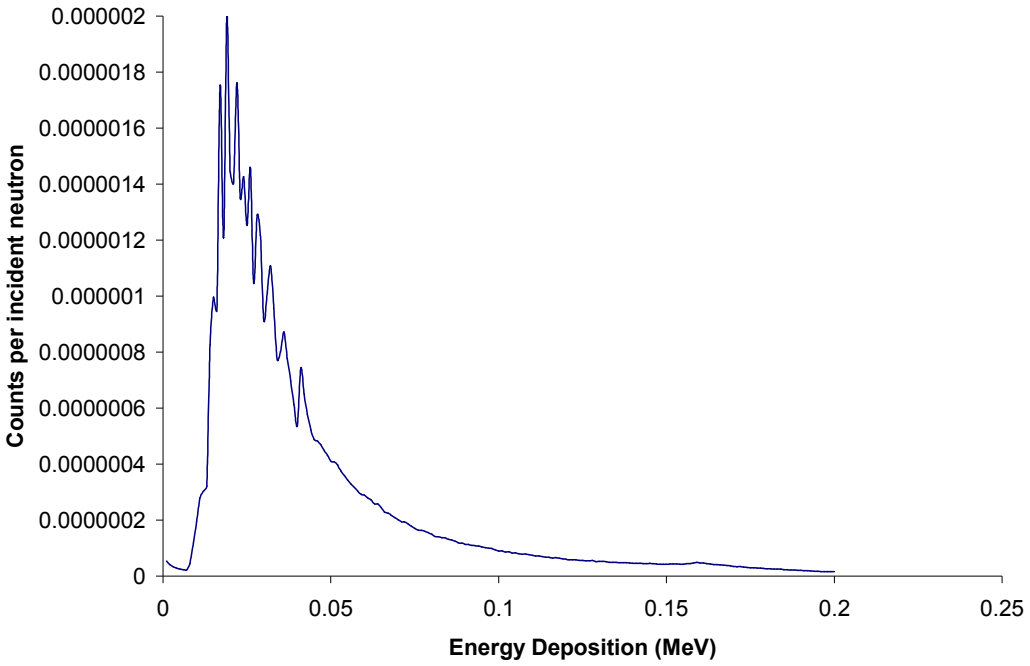

Figure 4.6. The simulated result of the detector's response to ^{252}Cf neutrons.

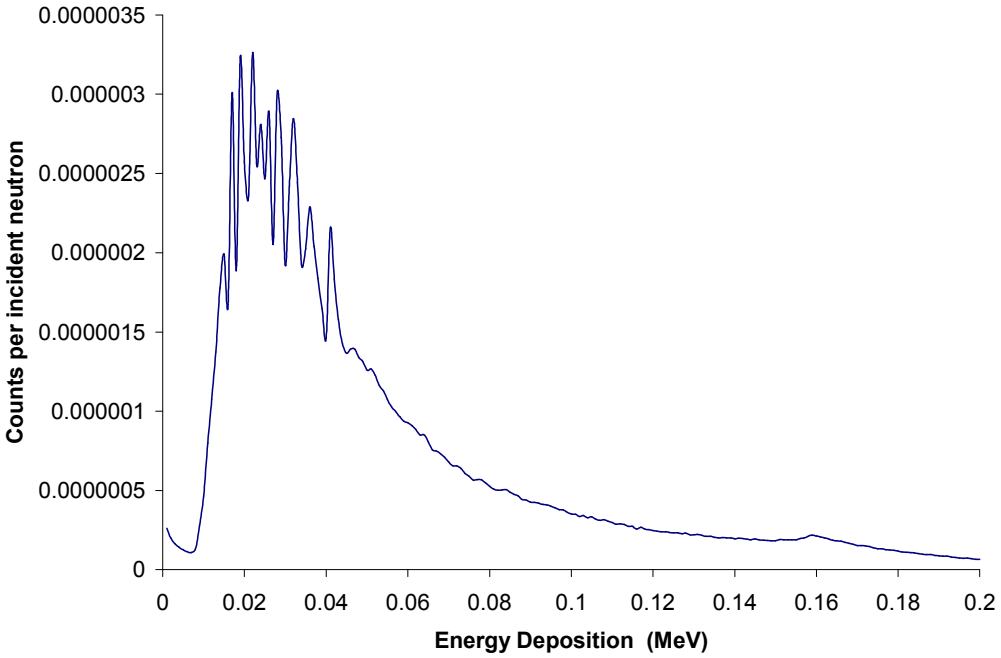

Figure 4.7. The simulated result of the detector's response to Am-Be neutrons.

4.2.3 Response to ^{137}Cs Gamma Rays

Because both ^{252}Cf and AmBe emit gamma rays and because the GEM-based TEPC is responsive to both neutrons and gamma rays, it is necessary to study the GEM-based TEPC for its ability to distinguish neutron events from the gamma-ray events. Monte Carlo Code MCNP was used to obtain the detector's response to gamma rays [33]. The photon source used in the MCNP calculation is that of ^{137}Cs – i.e. 661 keV monoenergetic photons.

The geometry in the MCNP calculation matches exactly the geometry of the detector used in the experiment (see the description in section 4.1). The energy distribution was obtained with the *F8 tally. The MCNP input file is provided in Appendix B.1. Figure 4.7 shows the result of the MCNP calculation.

As shown, the energy deposition for the gamma-ray events is significantly smaller than the energy depositions for the neutron events. This is expected because the gamma-ray events have lower LET than that of neutron events. The distinctly different energy deposition distribution, therefore should allow the GEM-based TEPC to distinguish neutron events from gamma-ray events.

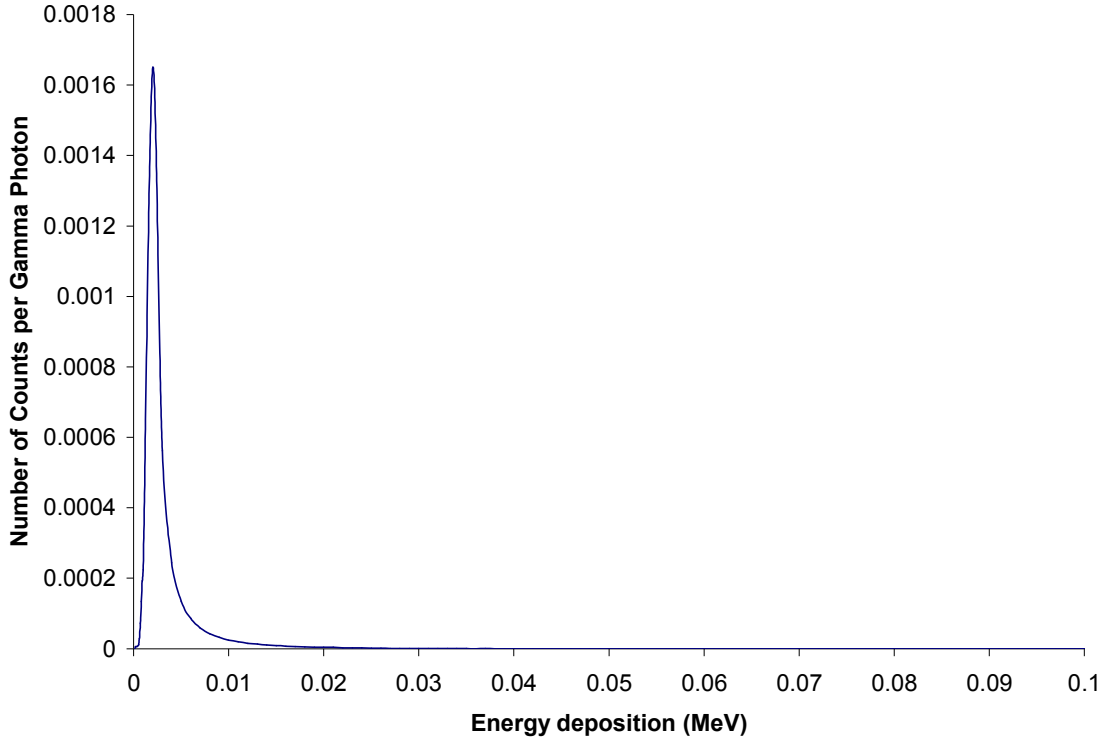

Figure 4.8. The simulated result of the detector's response to gamma rays emitted from ^{137}Cs.

4.3 Response as a Neutron Rem Meter

In order for a GEM-based TEPC to be used as a neutron Rem meter, it is necessary for the detector to have a response function that closely resembles the curve of $H^*(10)$ – vs. neutron energy (see Fig.4.9). Because different nuclear reactions are responsible for the TEPC's response to neutrons with energies above and below 0.5 MeV, it is necessary to obtain the simulated result separately for neutrons with energies above and below 0.5 MeV. For neutrons with energies above 0.5 MeV, the TEPC's response is caused by recoil protons originating in A-150 and it can be directly obtained from Fig. 4.3. A quick evaluation, however reveals that for neutrons with energies above 0.5 MeV the TEPC's response increases with neutron energy at a much greater extent than how $H^*(10)$ increases with neutron energy. Since it was noted in section 4.2.1 that the energy deposition in the TEPC decreases as neutron energy increases, setting an energy deposition threshold (with pulse height discriminator) would suppress the response of high-energy neutrons and make the TEPC's response curve match better with the $H^*(10)$ vs. neutron energy curve.

Figure 4.10 shows the simulated neutron response curves of the GEM-based TEPC for the various energy deposition thresholds. These curves were obtained from Fig. 4.3 by integrating the counts that have energy depositions above the corresponding threshold value. As shown, the curve corresponding to the threshold energy of 15 keV best matches the $H^*(10)$ curve. Figure 4.10 also shows that the detector's response due to the recoil protons originating in A-150 drastically diminishes for neutrons with energies below 0.5 MeV.

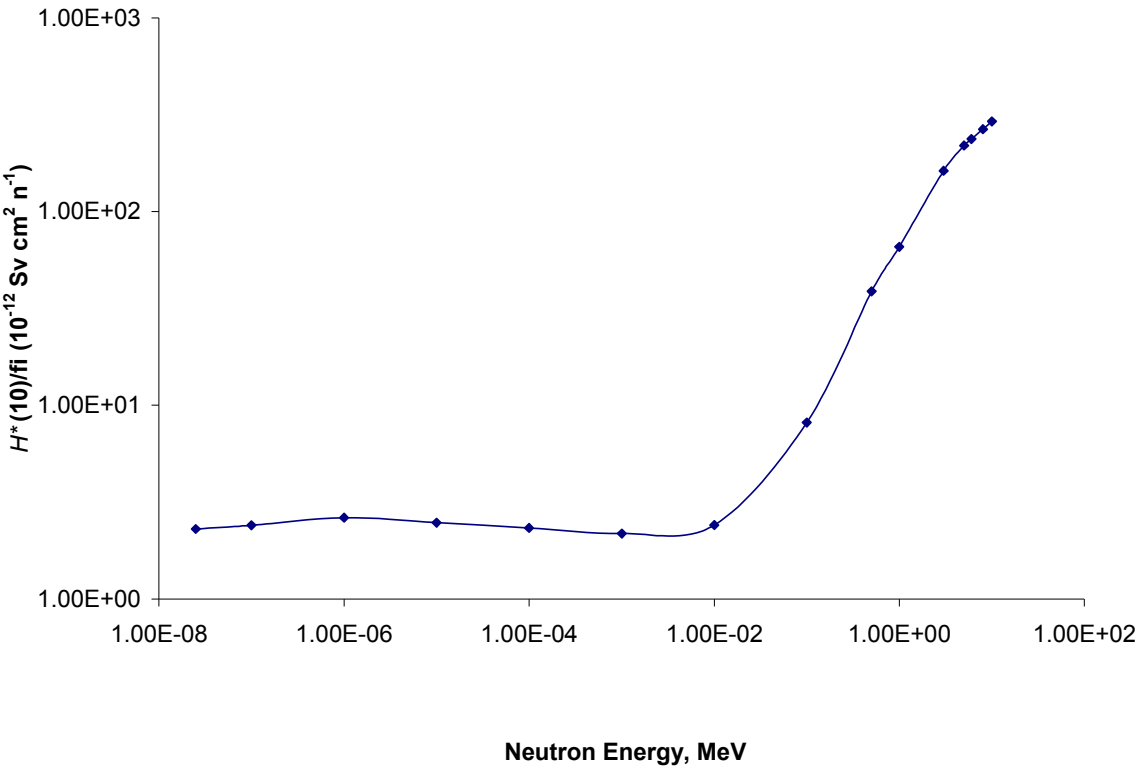

Figure 4.9. Ambient dose equivalent $H^*(10)$ per unit fluence [23].

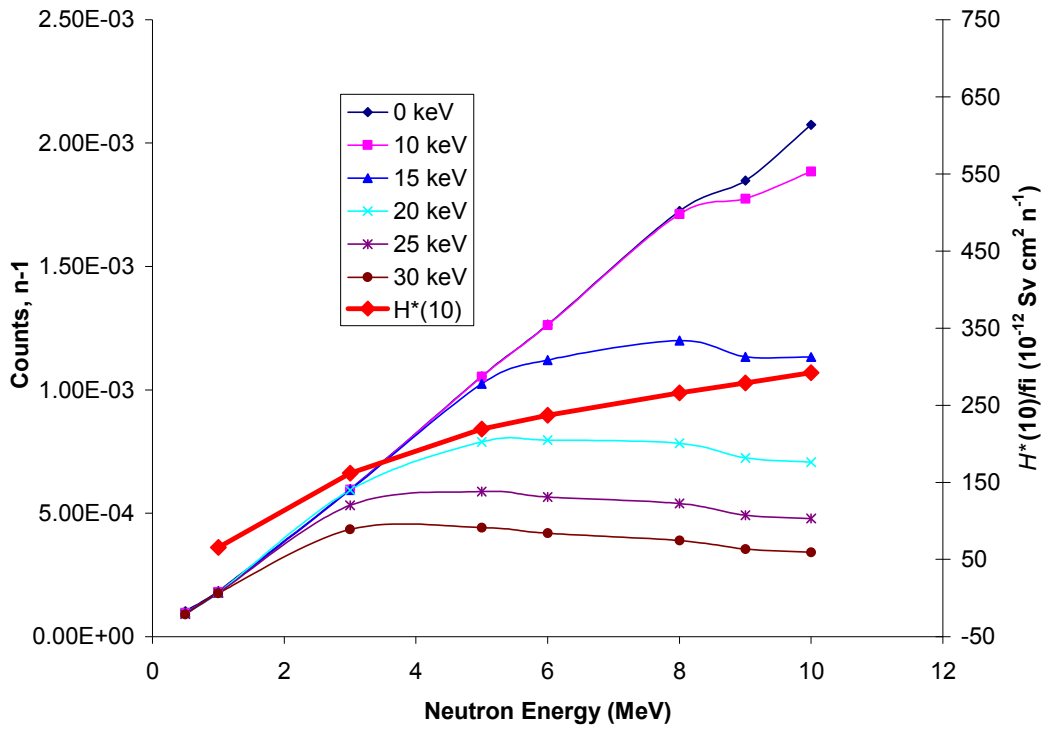

Figure 4.10. The neutron response function of the GEM-based TEPC due to the recoil protons originating in the A-150 for various thresholds of energy deposition.

For neutrons with energies below 0.5 MeV the TEPC's response is mainly caused by the $^{14}N(n,p)^{14}C$ reaction occurring in the gas region. In this case, the MCNP code was used to generate the $^{14}N(n,p)^{14}C$ reactions in the gas region of the TEPC. The MCNP input file is provided in Appendix B.2. As shown, tally type F6 was used to first obtain the neutron kerma, which was then divided by 620 keV (the Q value for the $^{14}N(n,p)^{14}C$ reaction) to obtain the number of $^{14}N(n,p)^{14}C$ reactions occurring in the gas region. The gas mixture used in the MCNP calculation was based on 1/3 atm of nitrogen and 1/3 atm of p-10. The simulated result is shown in Fig.4.11. As shown, the TEPC's response due to $^{14}N(n,p)^{14}C$ reactions decreases as neutron energies increase. Consequently, the combination of Figures 4.10 and 4.11 show that the detector lacks the response for neutron energy between 1 keV and 100 keV.

For the intermediate energy range, however, the recoil protons originating in the P-10 gas become significant contributors. By combining Figures 4.10 and 4.11 and by including the contributions of recoil protons originating in the P-10 gas, one may produce a complete neutron response curve (see Figure 4.12) that matches reasonably well with the $H^*(10)$ curve.

Figure 4.13 further demonstrates how well the two curves in Fig 4.12 match. It is obtained by dividing the response curve of the GEM-based TEPC by the $H^*(10)$ curve. The ideal response curve of a neutron Rem meter would be a straight horizontal line, which means the detector's response is completely independent of neutron energy, and therefore the total counts recorded by the detector can be directly converted to $H^*(10)$. The response curve shown in Fig. 4.13 is actually flatter (i.e. better) than all the response curves of the commercially available neutron Rem meters [27, 35-37].

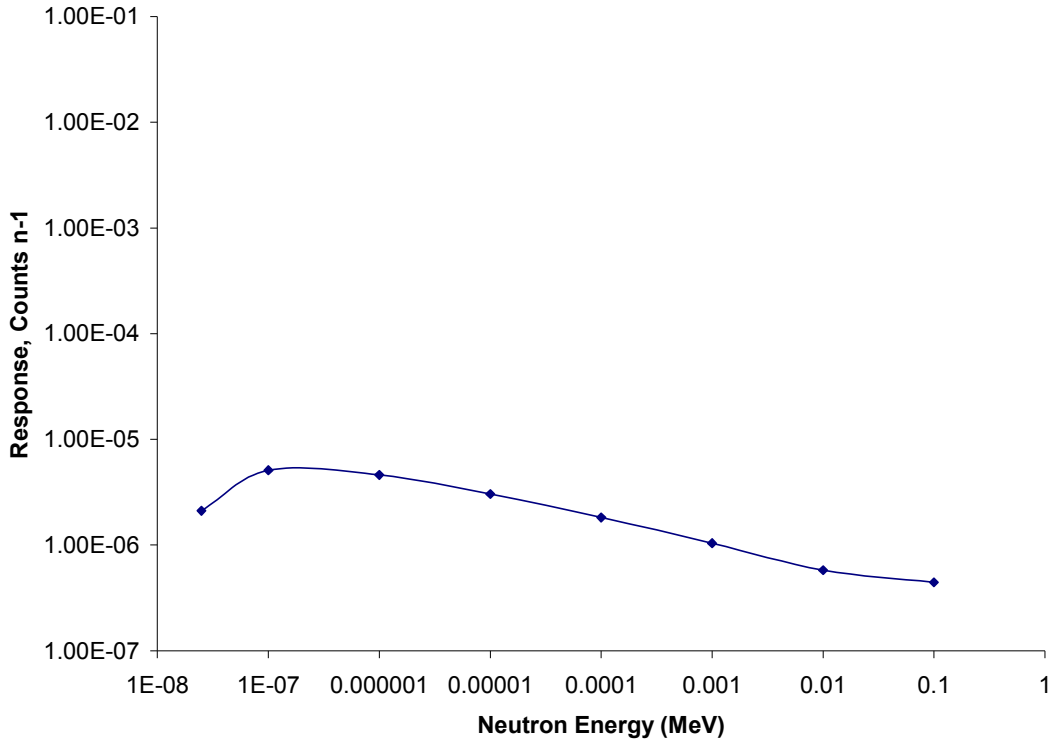

Figure 4.11. The simulated neutron response curve of the GEM-based TEPC due to the $^{14}N(n,p)^{14}C$ reactions.

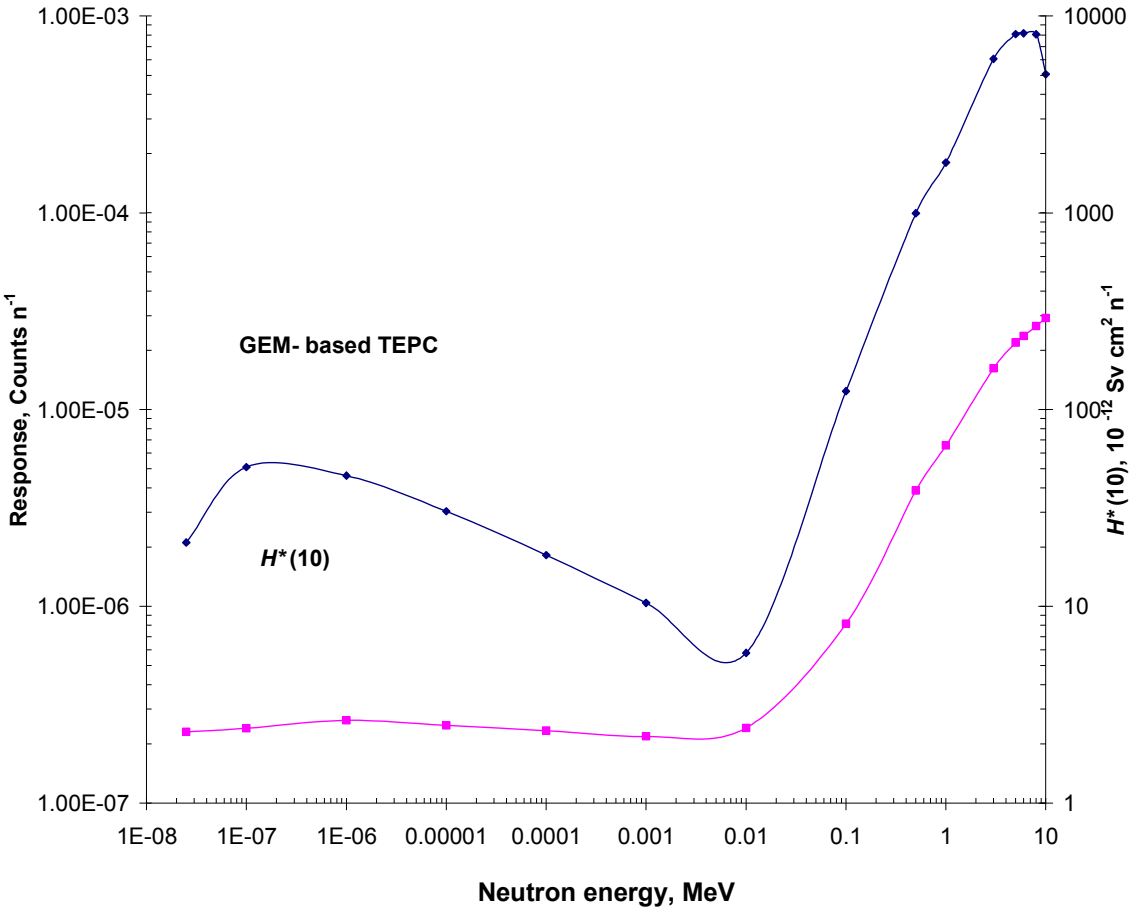

Figure 4.12. The comparison of the simulated neutron response curve of the GEM-based TEPC with the $H^*(10)$ curve.

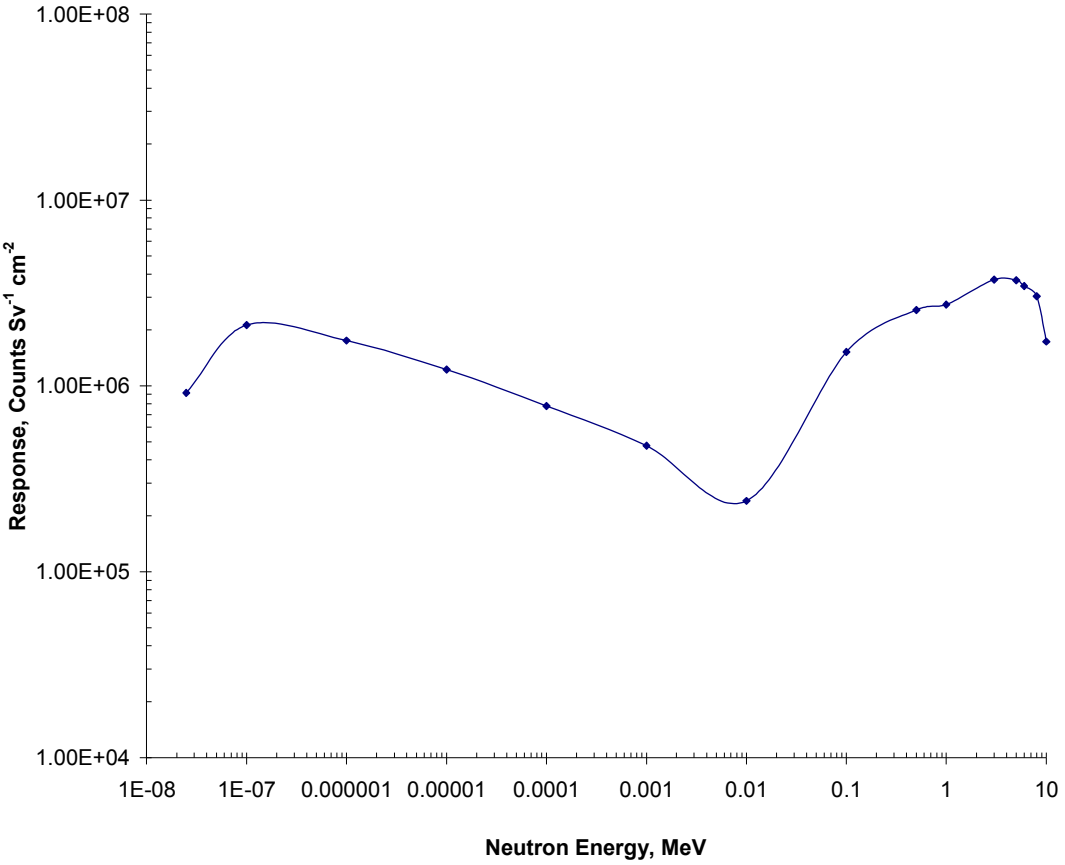

Figure 4.13. The simulated response per unit $H^*(10)$ as a function of neutron energy for the GEM-based TEPC.

According to Fig. 4.13, the sensitivity of the GEM-based TEPC for a bare ^{252}Cf neutron source was calculated to be 1.1 cpm per μSv h^{-1}, which is smaller than the sensitivity of the PRESCILA neutron probe [35]. However, as mentioned earlier, one can increase the sensitivity many times by stacking several GEM-based TEPCs together in one unit and by increasing the surface area of the detector. The neutron response of a stacked unit should be directly proportional to the number of GEM-based TEPCs in the unit. Taking the detector's weight into consideration, it can be shown that a stacked unit of five GEM-based TEPCs would still weigh less than 2 kg.

CHAPTER 5

EXPERIMENTAL METHODS

5.1 Gas Flow System

Several experiments have been performed using the GEM-based TEPC described in Chapter 3. The neutron and gamma-ray sources used in the experiments are the same as those used in the simulations, i.e. ^{252}Cf, AmBe and ^{137}Cs (see Chapter 4). The detailed description of the experimental setups and procedures are provided below.

One very important aspect for proper operation of the GEM-based TEPC is the gas quality which includes gas purity and stability of gas pressure. On one hand, a small contamination of the gas with electronegative gases, e.g. oxygen and water vapor, may significantly reduce the charge collection. On the other hand, variations in gas pressure may cause significant fluctuation of the electron multiplication of GEM (and thus the energy deposition distribution of the measured results). Gas impurities may be caused by gas leakage and outgassing of plastic components and glue. Since outgassing is very difficult to avoid, it is preferable to use a gas flow system so that it provides continuous flow of the high-purity gas with a steady pressure.

Two types of gas were used in the experiments: the P-10 and the propane-based tissue-equivalent (TE) gas. The measurements using the P-10 gas were made with the pressure set at 1 atm. Whereas, the measurements using the propane-based TE gas were conducted below 1 atm. This is because a report [38] shows that the optimal electron multiplication of the GEM occurs at 0.3 atm for the propane-based TE gas. In order to maintain the leaky detector at a steady gas pressure significantly below 1 atm, it was necessary to build a gas flow system with a vacuum pump and a buffer chamber.

The gas flow system used is schematically illustrated in Fig. 5.1. As shown, the "buffer chamber" sits between the TEPC and the vacuum pump, and it has enough volume to minimize the pressure surge caused by the operation of the vacuum pump. The buffer chamber is made of PVC (polyvinyl chloride). The gas flow meter (LUDLUM - 2750) was used to measure the gas flow through the detector.

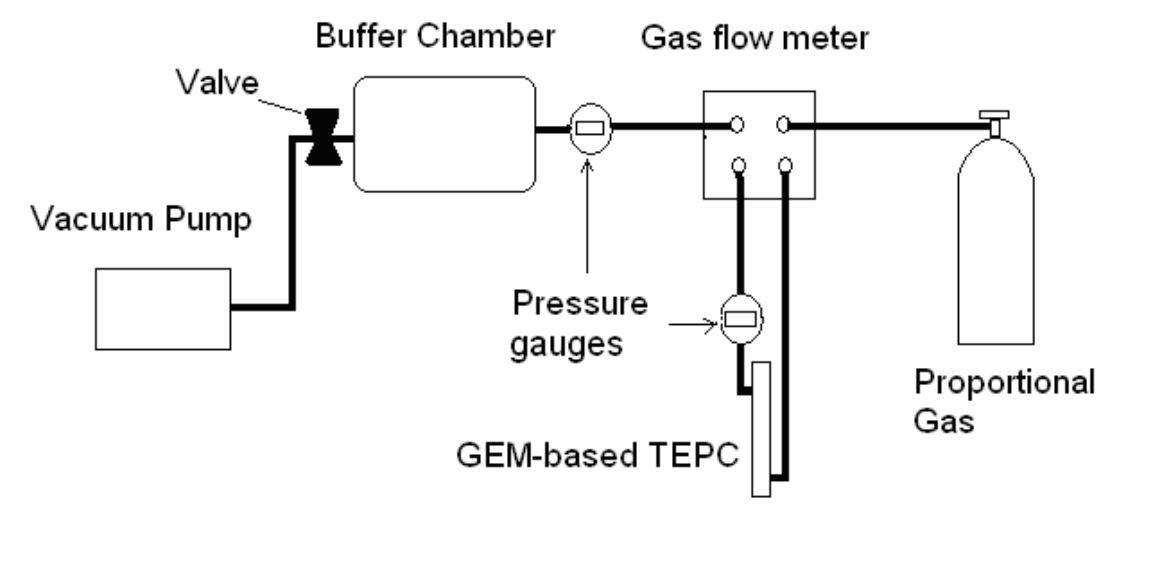

Figure 5.1. Schematic diagram of the gas flow system used with the GEM-based Tissue-Equivalent Proportional Counter (TEPC).

5.2 Electronics and Signal Processing

The GEM-based TEPC was operated in the pulse mode to record each individual energy deposition event. The output voltage pulse is proportional to the charge released in the gas cavity due to an event. A low-noise charge-sensitive preamplifier – ORTEC - 142 PC was used to collect the charge and to convert it to voltage pulse which is, in turn, amplified and shaped by a linear amplifier CANBERRA-202. The voltage pulses coming out of the linear amplifier were then sent to the multichannel analyzer (MCA) where they were converted to digital signals for recording and display. The MCA is equipped with a lower level discriminator (LLD) that may be used to prevent the low-level noise signals from entering the MCA and jamming the analog-to-digital conversion process. Fig. 5.2 shows the signal processing units used for the experiments. As shown, the high voltage (HV) power supply CANBERRA 3002D used to bias the TEPC was connected via the preamplifier.

There are two possible ways in which the preamplifier and the bias voltage can be connected to the detector.

1. to hold the detector wall at ground potential and apply a positive high voltage to the anode, and
2. to apply negative high voltage to the detector wall and hold the anode at ground potential.

The first configuration has the advantage that the wall does not need to be insulated as in the second configuration. The advantage of the second configuration is that it eliminates the high voltage and blocking capacitor which reduces the total input capacitance. In this study the first method was used. It was chosen because of its safety.

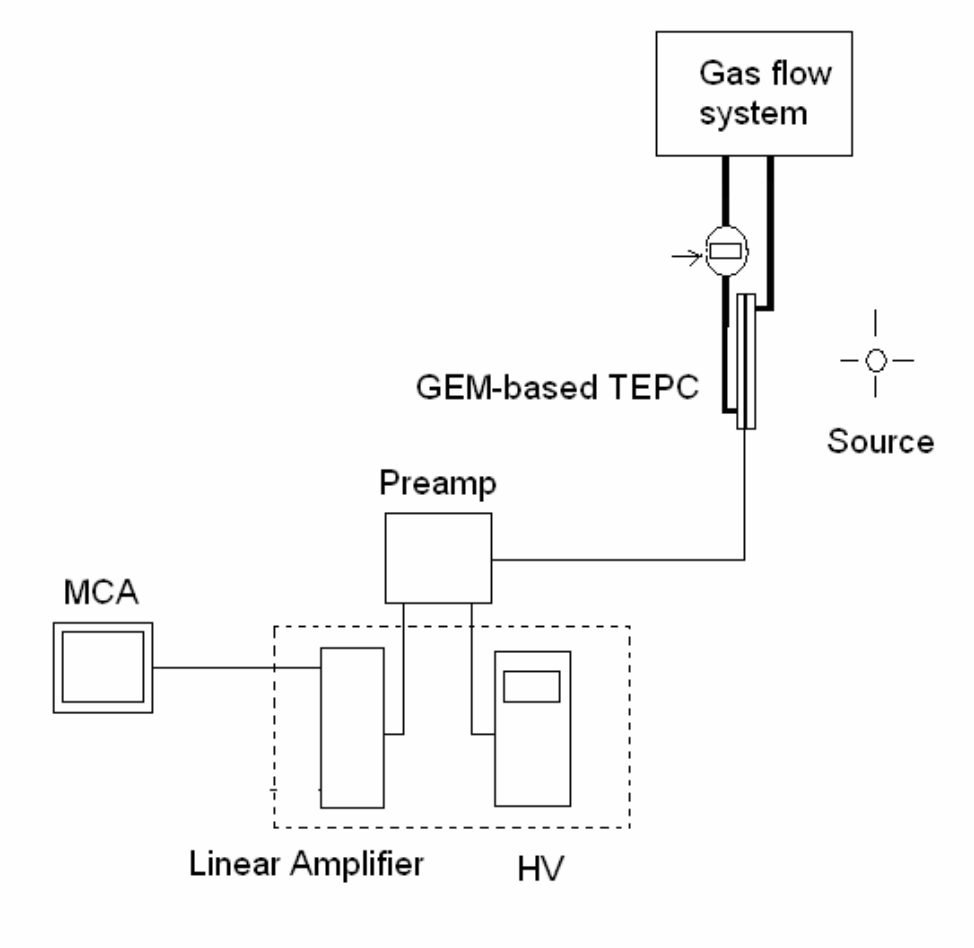

Figure 5.2. Experimental setup with the signal processing units.

5.3. Description of the Experiments

All experiment were conducted in the mezzanine of the High Bay in the Neely Nuclear Research Canter at Georgia Tech. The mezzanine has dimensions 11.5 m × 6 m × 20 m. The actual experimental area is 6.3 m ×5.5 m as shown in Fig. 5.3. A concrete wall 2.5 m high and 5.5 m long was set up to separate and shield the experimenter's designated area from the experimental area. Fig. 5.4 shows a picture of the electronics and signal processing equipment. Fig.5.5 shows the detector in the radiation area.

Experiments were conducted using the ^{252}Cf and AmBe neutron sources, and the ^{137}Cs gamma-ray source. Both the P-10 gas and the propane-based TE gas were used for the measurements. The GEM-based TEPC was fixed on a stand (Fig 5.5). The source-to-detector distance was 5 inches (see Fig.5.3).

The P-10 gas was used at a pressure of 1 atm. The propane-based TE gas was used at several different pressures below 1 atm. For tests conducted using pressure of 1 atm, there was no need to run the vacuum pump and the buffer chamber. That is, the vacuum pump and buffer the chamber were used only for gas pressure below 1 atm. The gas distribution system was able to achieve a pressure as low as -14.5 psig (or 0.2 psia), and to hold this pressure with an accuracy of 0.01 psi.

It should be mentioned that P-10 gas pressures below 1 atm were also used but quickly dismissed because the electron multiplication of the GEM became so high that the results became unreliable. The experimental procedure for the measurements using the P-10 gas is outlined below.

1. Connect the detector and data acquisition system as shown in Fig. 5.2.
2. Open the valve of the P-10 gas cylinder so that the gas pressure does not exceeds 20 psi, which is the maximum input pressure for the gas flow meter.
3. Set the gas flow with the gas flow meter to 20 cm^3/min which is the minimum flow rate required to suppress the leakage current across the GEM.
4. Set the voltage on HV power supply to 700 V, which corresponds to 400 V across the GEM. This value was the minimum voltage when signal became observable on the oscilloscope.
5. Record the pulse height spectrum with the MCA for 20 minutes.
6. Increase the voltage with an increment of 50 V and repeat step 5 until the voltage reaches 950 V, beyond which the GEM foil may be damaged.

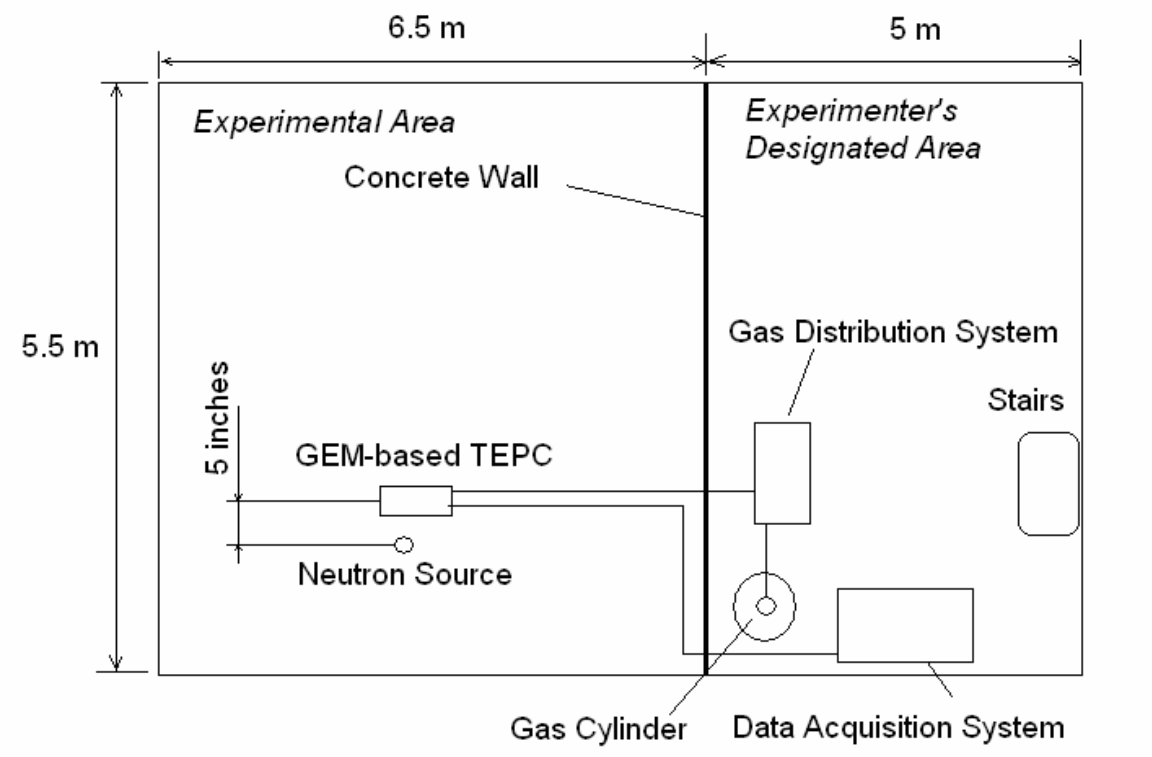

Figure 5.3. Diagram of the Experimental Setup in Mezzanine of the High Bay.

Figure 5.4. View of entire experimental setup.

Figure 5.5. GEM-base TEPC in the radiation area.

The measurements using propane-based TE gas at various pressures below 1 atm were far more complicated and time consuming than the measurements made at atmospheric pressure with the P-10 gas. The biggest challenge was to sustain the stable pressure in the detector. As shown in Fig. 5.2, two pressure gauges were used. One is connected directly to the GEM-based TEPC. The second one is connected to the buffer chamber. The reason for having two pressure gauges was to precisely control the pressure inside the detector. This is further explained as follows. As shown in Fig 5.3, the GEM-based TEPC was placed inside the brick wall in the mezzanine, whereas the data acquisition system and the gas distribution system were outside the brick wall in the experimenter's designated area. In other words, during experiments only the pressure gauge that is connected to the buffer chamber can be observed. A set of measurements was made without the radiation source to find the relationship between the pressure in the buffer chamber and the pressure in the detector. The results are presented in Table 5.2. From the data presented in Table 5.2 the relationship between the two pressures can be found:

$$p_d = 0.9463 \cdot P_b + 0.1953 \tag{5.9}$$

Where p_d is the pressure in the detector, and p_b is the pressure in the buffer chamber. To sustain the stable pressure in the system, the gas distribution system uses two control valves (see Fig.2). One valve is connected to the vacuum chamber, and it controls the gas outflow. The second valve is part of the gas flow meter, and it controls the gas inflow. In order to achieve a stable low pressure, it was necessary to adjust tboth valves so that the inflow matched the outflow. The stability of the pressure achieved during the experiment was ±0.01 psi. The nominal gas flow rate was 20 cm^3/min.

Table 5.2. Correlation between pressure in the buffer chamber and that in the GEM-based TEPC.

Pressure in the buffer chamber, psig	Pressure in the GEM-based TEPC, psig
-14.5	-13
-13.82	-12.42
-13	-12
-12	-11.24
-11	-10.36
-10	-9.45
-9	-8.49
-8	-7.51
-7	-6.54
-6	-5.58
-5	-4.57
-4	-3.58
-3	-2.56
-2	-1.57
-1	-0.59

The experimental procedure for the measurements using the propane-based TE gas is outlined as follows:

1. Connect the detector, data acquisition system and gas distribution system as shown in Fig. 5.2.
2. Open the valve of the TE gas cylinder so that the gas pressure does not exceeds 20 psi.
3. Turn on the vacuum pump.
4. Adjust the two valves connected to the buffer chamber and the gas flow meter to achieve and stabilize the desired pressure.
5. Set the voltage on HV power supply to 700 V, which corresponds to 400 V across the GEM. This value was the minimum voltage when signal became observable on the oscilloscope.
6. Record the pulse height spectrum with the MCA for 20 minutes
7. Increase the voltage with an increment of 50 V and repeat step 5 until the voltage reaches 950 V, beyond which the GEM foil may be damaged.
8. Repeat steps 4-7 for the various gas pressures.

CHAPTER 6

EXPERIMENTAL RESULTS

6.1. Pulse Height Distribution of the AmBe Source

Fig. 6.1 shows the pulse height distribution (PHD) of the AmBe source obtained with the GEM-based TEPC using P-10 gas at a pressure 1 atm and with several different voltages applied across the GEM. As shown, the voltages applied across the GEM cover a range between 400 volts and 550 volts. These distributions clearly show what is expected of a typical proportional counter, i.e. the pulse height increases as the detector's bias voltage increases. Figure 6.1 also shows that for the bias voltage of 550 volts, the spectrum is characteristic enough to allow neutron events to be separated from the gamma-ray events.

It should be noted that for bias voltages greater than 550 volts the increased gamma-ray event rate significantly increases the dead time of the data acquisition system and, therefore, causes the count rate to drop. Figure 6.2 shows the PHD obtained with the bias voltage of 550 volts in the linear scale so that the separation between neutron events and gamma-ray events is more clearly illustrated. Figure 6.2 also shows that the background event rate (i.e. w/o radiation source) was low enough to be ignored.

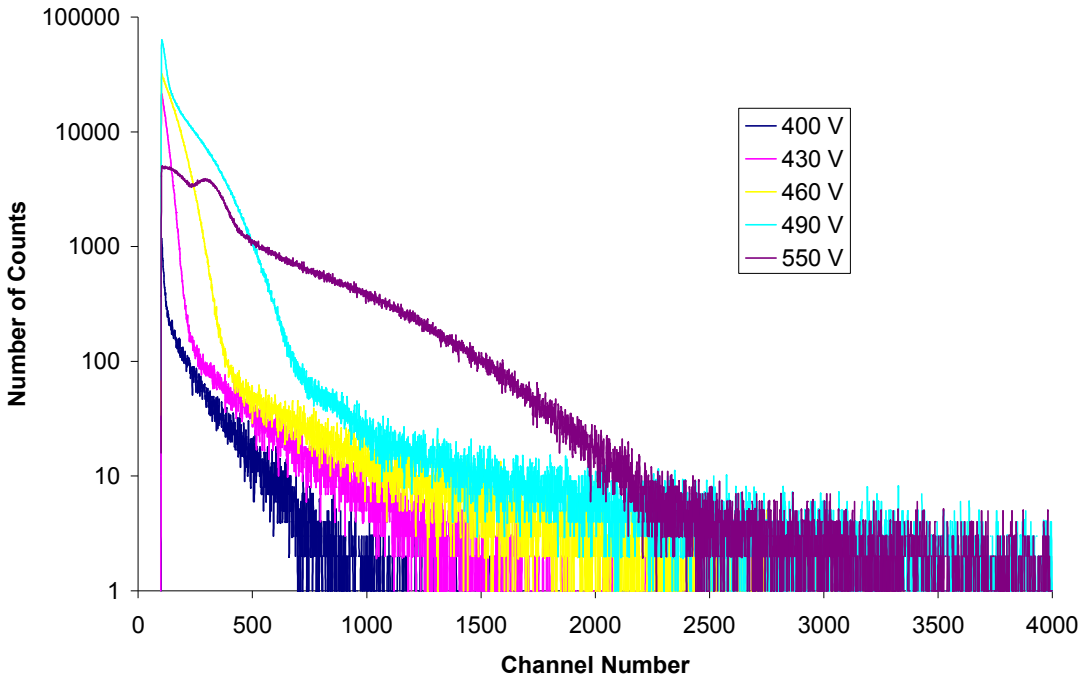

Figure 6.1. The Pulse-height distribution of AmBe source obtained with the GEM-based TEPC using 1 atm of P-10 gas, and with various bias voltages.

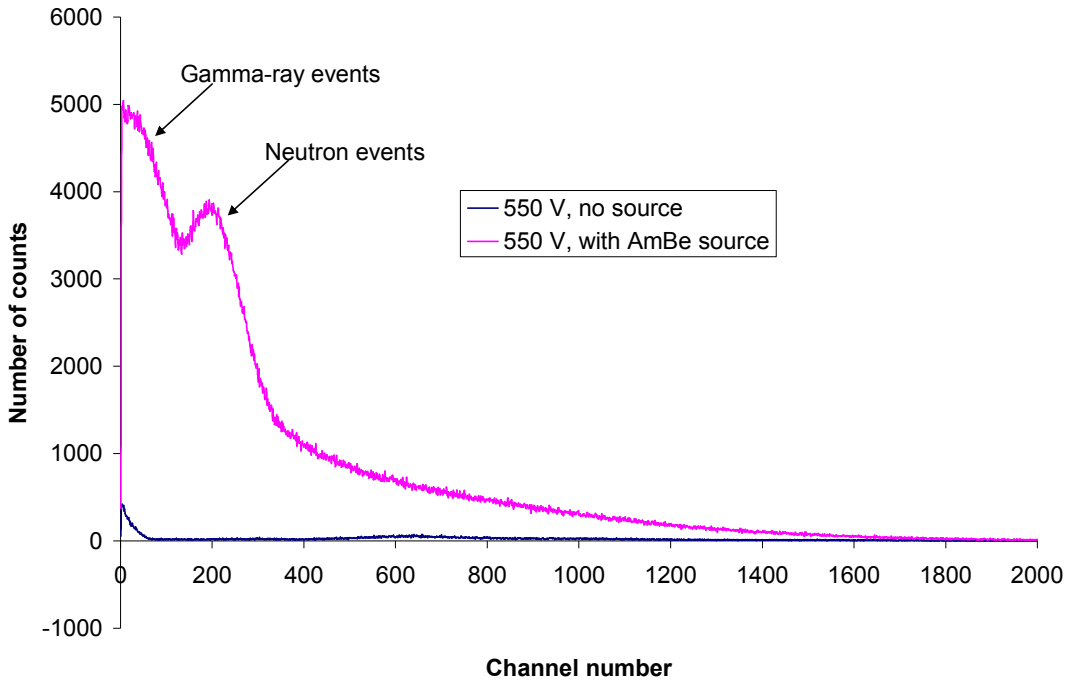

Figure 6.2. The pulse height spectrum of AmBe source obtained with the bias voltage of 550 volts.

6.2. Pulse Height Distribution of the ^{252}Cf Source

Fig. 6.3 shows the pulse height distributions of the ^{252}Cf source obtained with the GEM-based TEPC using 1 atm of P-10 gas and with several different voltages applied across the GEM.

This figure is consistent with Figure 6.1 in that there is a range of bias voltages within which pulse height increases as the voltage increases. But the increase of the dead time of the system for the higher voltages is more pronounced than for the AmBe source. This is probably because the ^{252}Cf source produces more gamma-ray events than are produced by the AmBe source. Figure 6.3 also shows that the PHD for bias voltage of 490 volts is the most characteristic for allowing neutron events to be separated from gamma-ray events. An optimal voltage of 490 volts was therefore chosen for the ^{252}Cf measurements. Figure 6.4 shows that the ^{252}Cf PHD obtained with 490 volts in the linear scale.

6.3. Pulse Height Distribution of the ^{137}Cs Source

Figure 6.5 shows the PHDs of the ^{137}Cs source obtained with the GEM- based TEPC using 1 atm of P-10 gas and with several bias voltages. When compared with Figures 6.1 and 6.3, Fig.6.5 clearly confirms that the gamma-ray events, in general, have smaller pulse heights than those of the neutron events. This sharp drop of count rates at large pulse heights is better illustrated in Fig.6.6, which is the same curve as the one shown on Fig.6.5 for 550 volts, except that it is plotted in the linear scale.

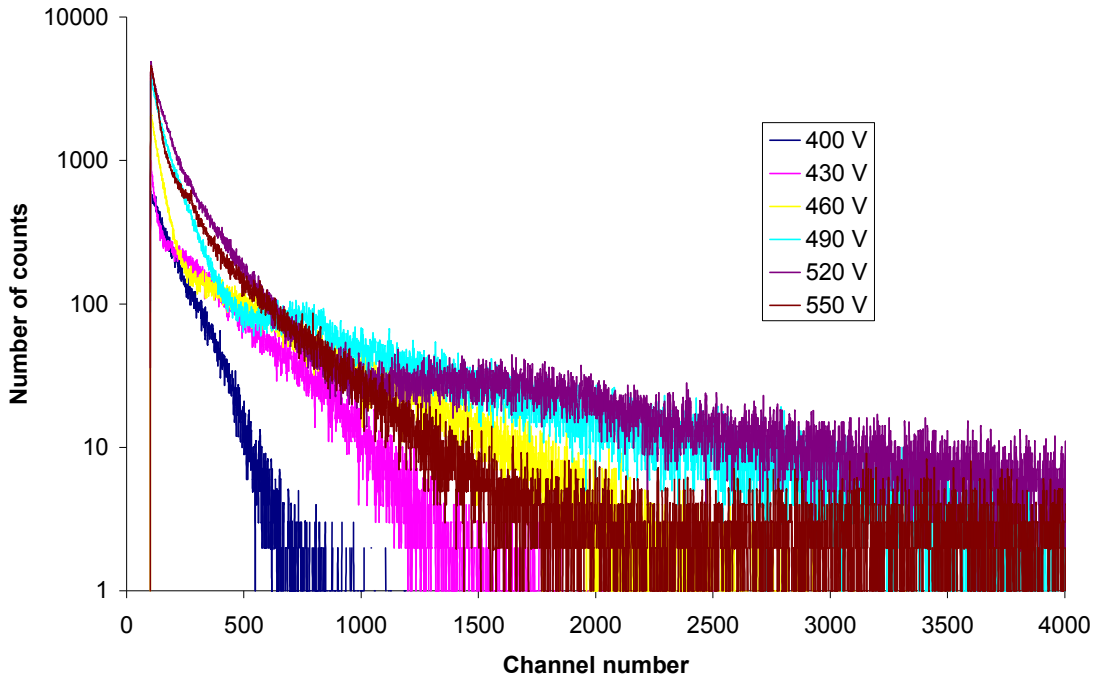

Figure 6.3. The pulse height distributions of ^{252}Cf source obtained with the GEM-based TEPC using 1 atm of P-10 gas, and with various bias voltages.

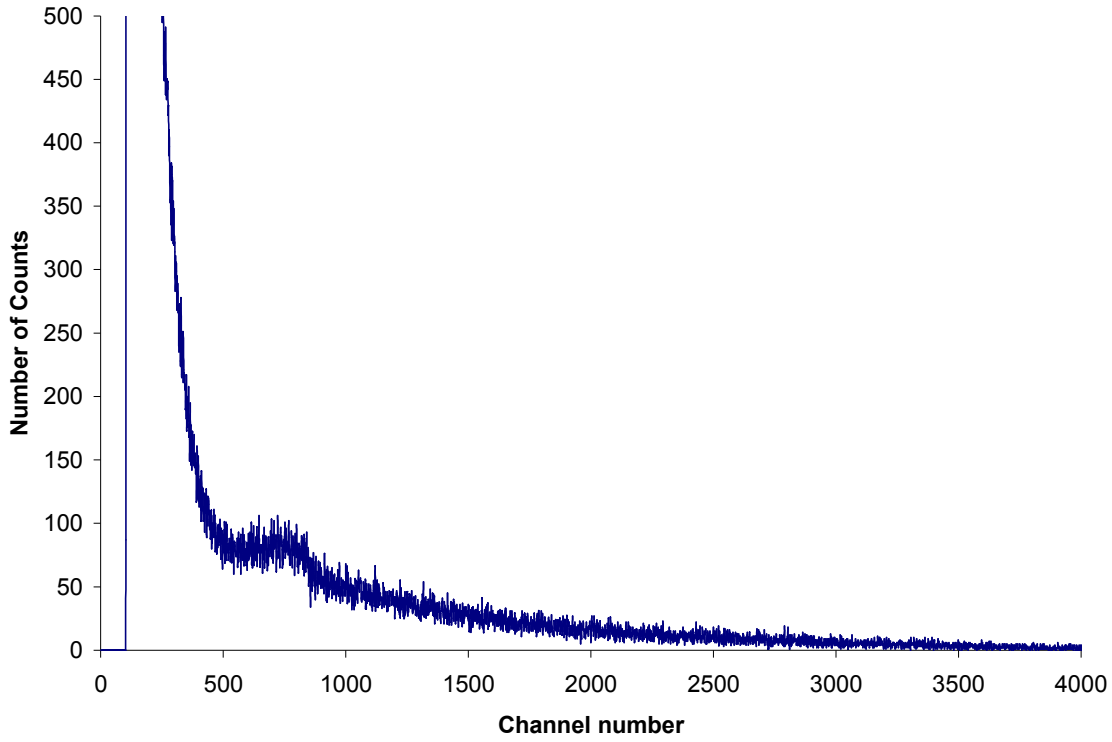

Figure 6.4. The pulse height distribution of the ^{252}Cf source obtained with the bias voltage of 490 volts.

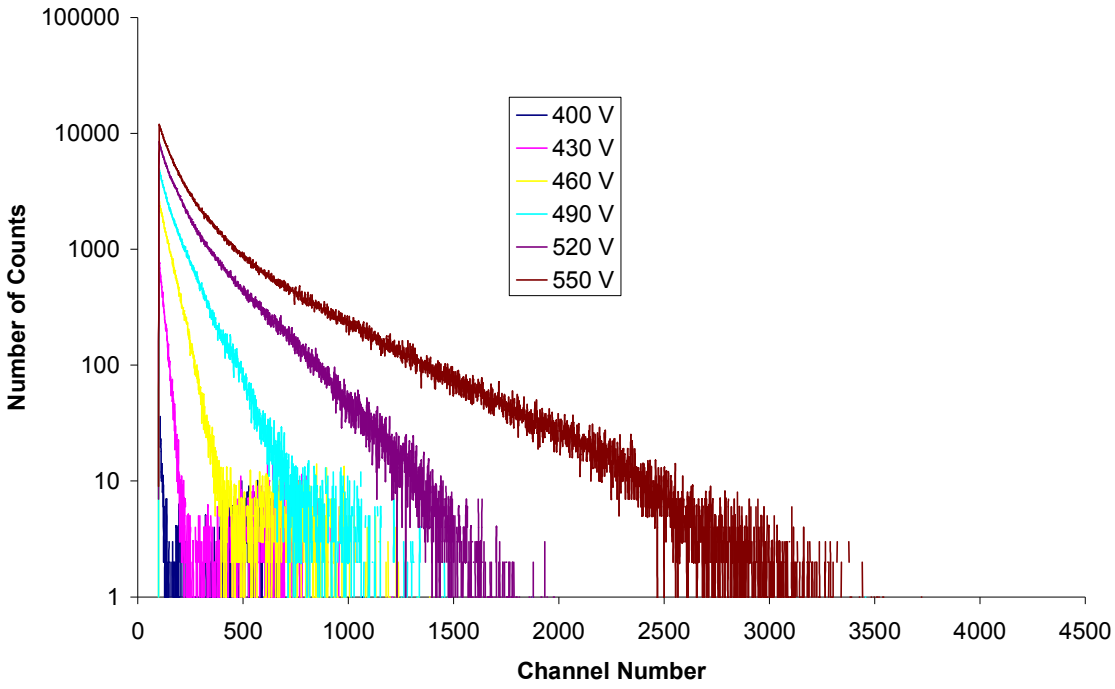

Figure 6.5. Pulse-height spectrum of ^{137}Cs source measured with the new GEM-based TEPC at a pressure 1 atm of P-10 gas for voltages on GEM 400 V-550 V.

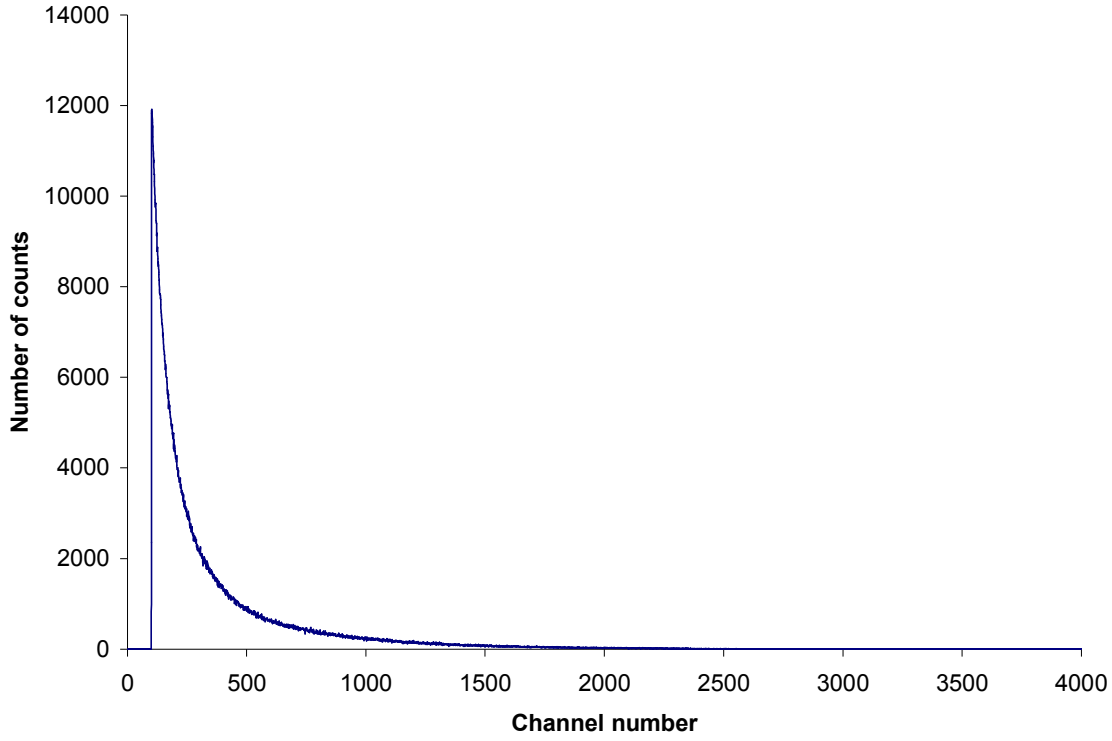

Figure 6.6. The pulse height distribution of the ^{137}Cs source obtained with the bias voltage of 550 volts.

6.4. Pulse Height Versus Gas Pressure

The propane–based TE gas was used to investigate how the electron multiplication factor of the GEM varies with gas pressure. The PHDs were obtained for each radiation source with the TEPC operated at two different pressures: 0.3 atm and 0.5 atm. Figures 6.7 -6.9 show the PHDs for the AmBe source, the ^{252}Cf source, and the ^{137}Cs source, respectively. All three figures were obtained with the bias voltage set at 550 volts. These figures show that the pulse height increases dramatically as the pressure reduces from 0.5 atm to 0.3 atm. Figure 6.7 additionally shows that the energy resolution worsens as the pressure reduces rom 0.5 atm to 0.3 atm. These findings are consistent with those reported by others [39,40].

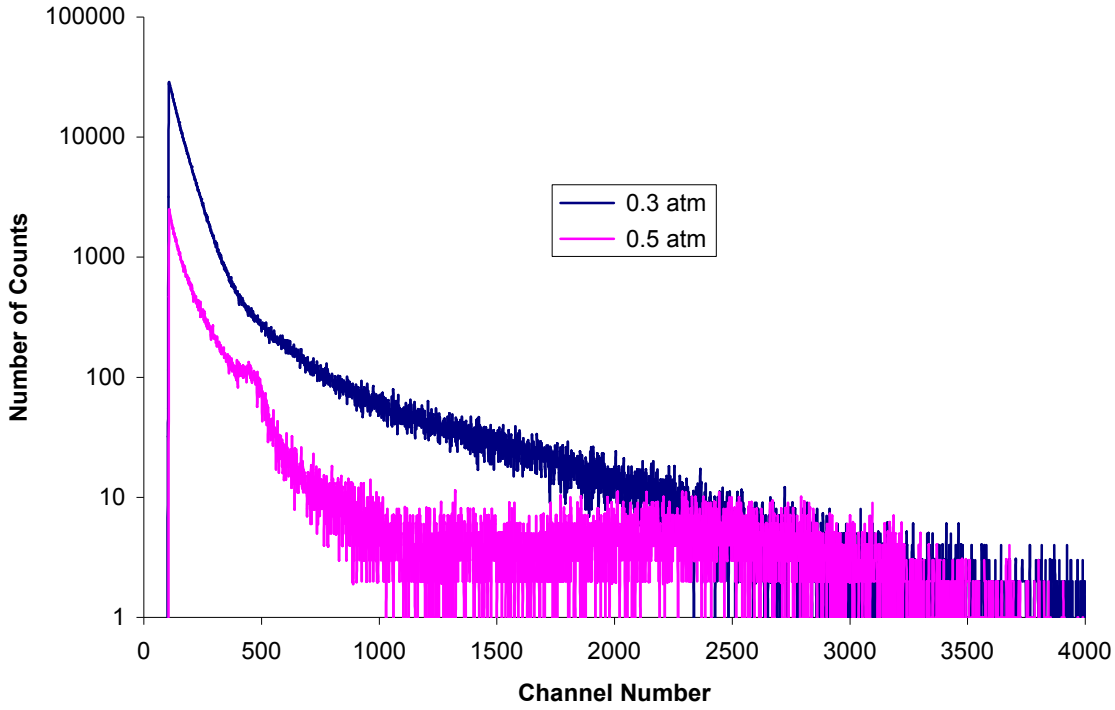

Figure 6.7. The pulse height distribution of the AmBe source obtained with the GEM-based TEPC filled with 0.3 atm and 0.5 atm of the propane-based TE gas.

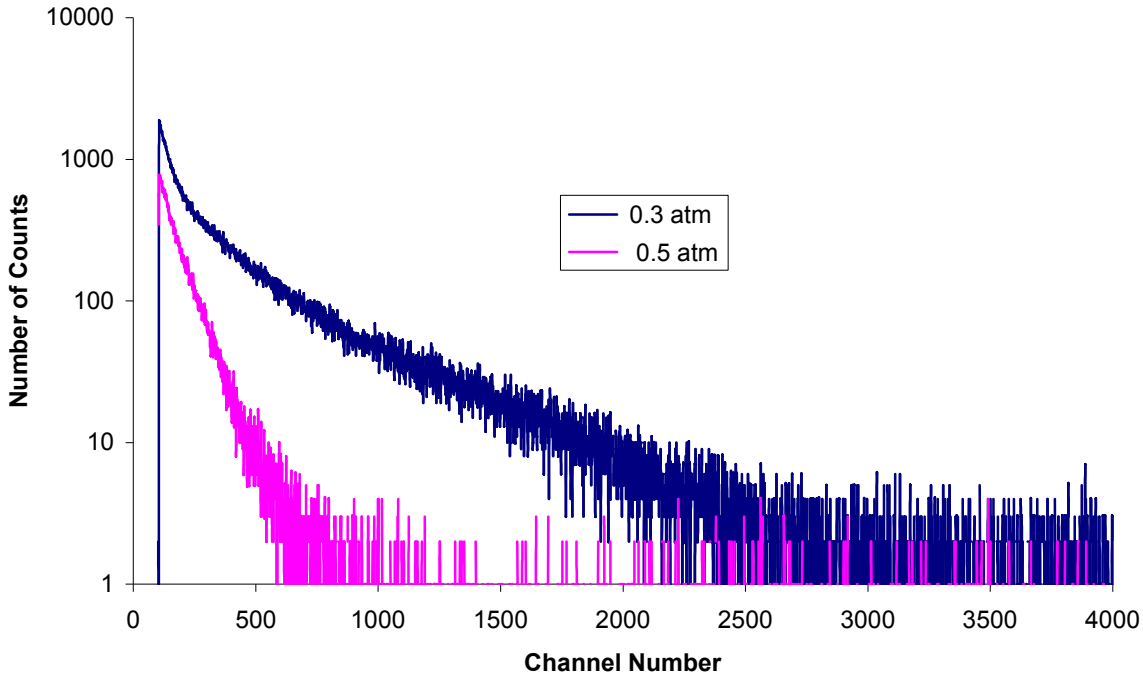

Figure 6.8. The pulse-height distribution of the ^{252}Cf source obtained with the GEM-based TEPC filled with 0.3 atm and 0.5 atm of propane based TE gas.

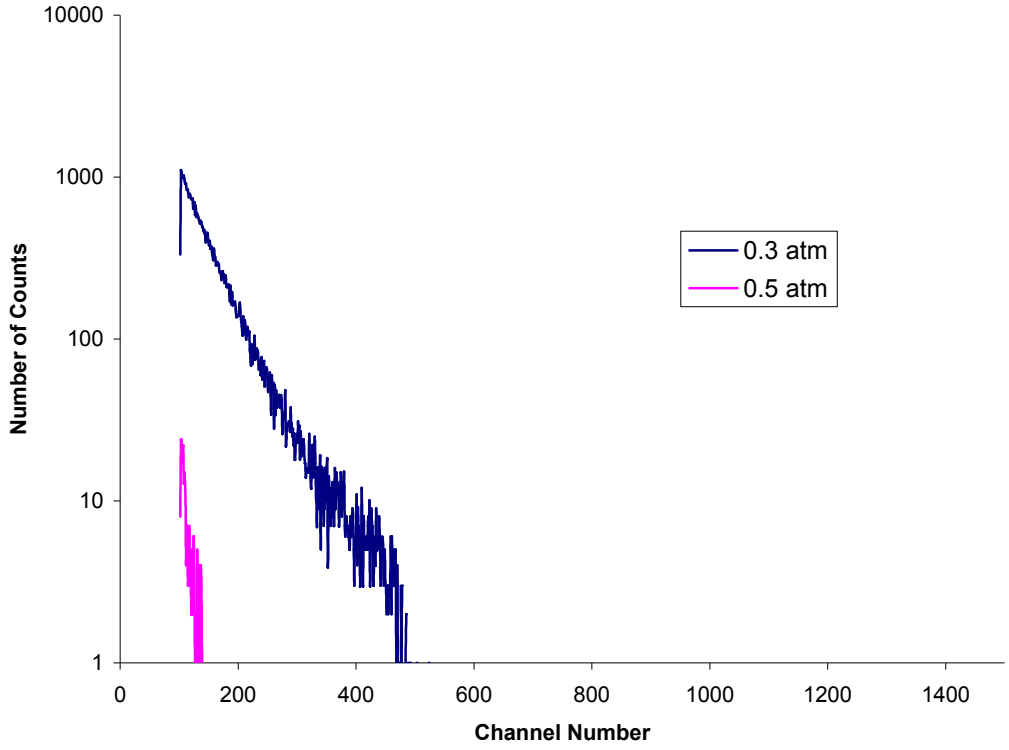

Figure 6.9. The pulse-height distribution of the ^{137}Cs source obtained with the GEM-based TEPC filled with 0.3 atm and 0.5 atm of propane based TE gas.

6.5. Comparison with the Simulated Results

In order to compare the measured results with the simulated results (figures 4.6 and 4.7) one must remove the gamma-ray events from the measured results. Since it is not possible to completely separate neutron events from gamma-ray events, an approximation was made by subtracting the measured PHD of the ^{137}Cs source from the measured PHD of the AmBe and ^{252}Cf sources. Figure 6.9 shows the measured PHDs of the AmBe and ^{137}Cs sources, and the subtracted neutron PHD. The two measured PHDs were taken from Figures 6.2 and 6.6. Figure 6.10 shows the measured PHDs of the ^{252}Cf and ^{137}Cs sources, and the subtracted neutron PHD. The two measured PHDs were taken from Figures 6.4 and 6.5. Figures 6.11 and 6.12 show that the shapess of the two subtracted neutron PHDs match well with that of the two simulated neutron PHDs.

To quantitatively assess the agreement between the experimental results and the simulated results, one must also know the neutron incident rates during the experiments. The neutron incident rates, R, can be obtained approximately by the following formula:

$$R = \frac{Sa^2}{4\pi d^2} \tag{6.1}$$

where S is the neutron emission rate (n/s), *a*, the size of the GEM, and d, the distance between the source and the GEM-based TEPC. By applying equation 6.1 with S=1.22×10^8 n/s for AmBe and S=9.3×10^7 n/s for ^{252}Cf, and with a=5.08 cm and d=12.7 cm, one obtains the neutron incident rates of 1.55×10^6 n/s and 1.18×10^6 n/s for AmBe and ^{252}Cf, respectively. Since chapter 4 shows that the simulated results give 1.8×10^{-4} counts and 1.3×10^{-4} counts per incident neutron for AmBe and ^{252}Cf, respectively, the simulated count rates would be 279 counts/s and 153 counts/s. Based on the experimental data shown on Figures 6.12 and 6.13, the total measured counts are 312,420 counts for the AmBe source and 886,467 counts for the ^{252}Cf source. By dividing the neutron count rates by the measurement times of 20 minutes for the AmBe experiment and 2 hours for the ^{252}Cf experiment, one obtains the count rates of 260 counts /s and 123 counts/s, respectively. These results compare favorably with the simulated results.

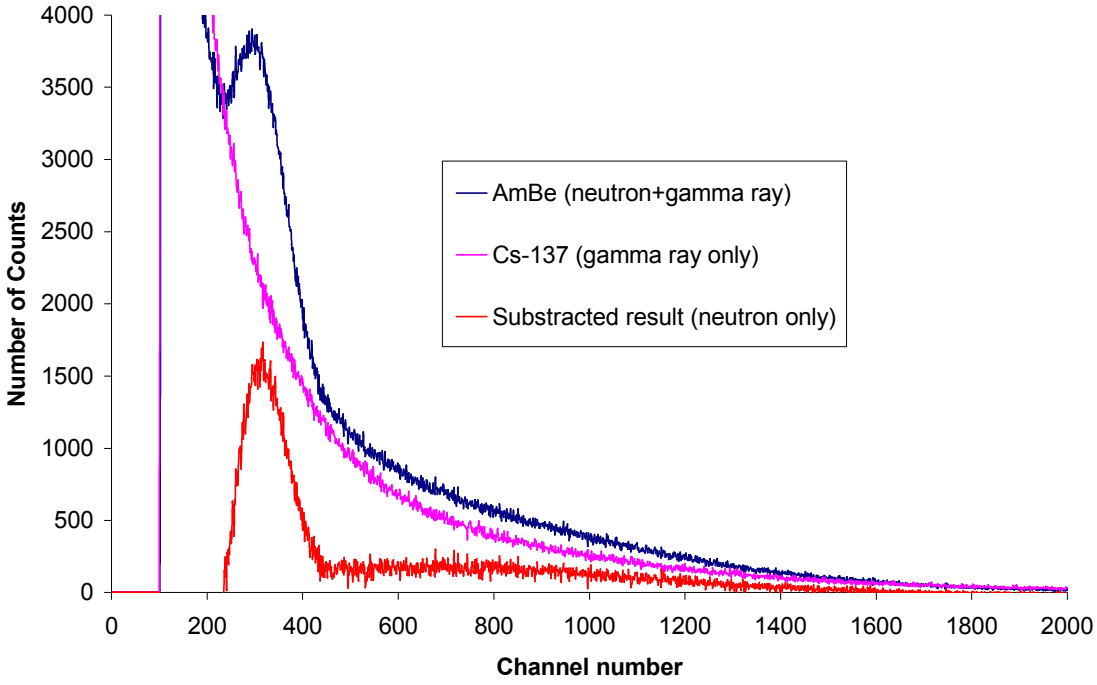

Figure 6.10. The measured PHDs of the AmBe and ^{137}Cs sources, and the subtracted neutron PHD.

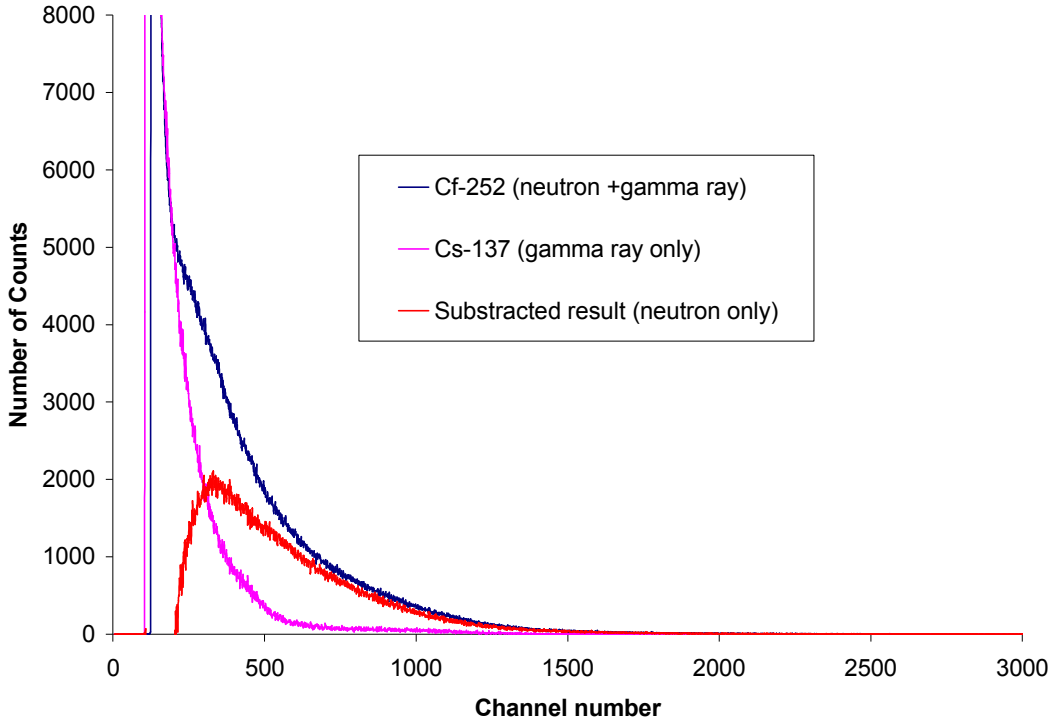

Figure 6.11. The measured PHDs of ^{252}Cf and ^{137}Cs sources, and the subtracted PHDs.

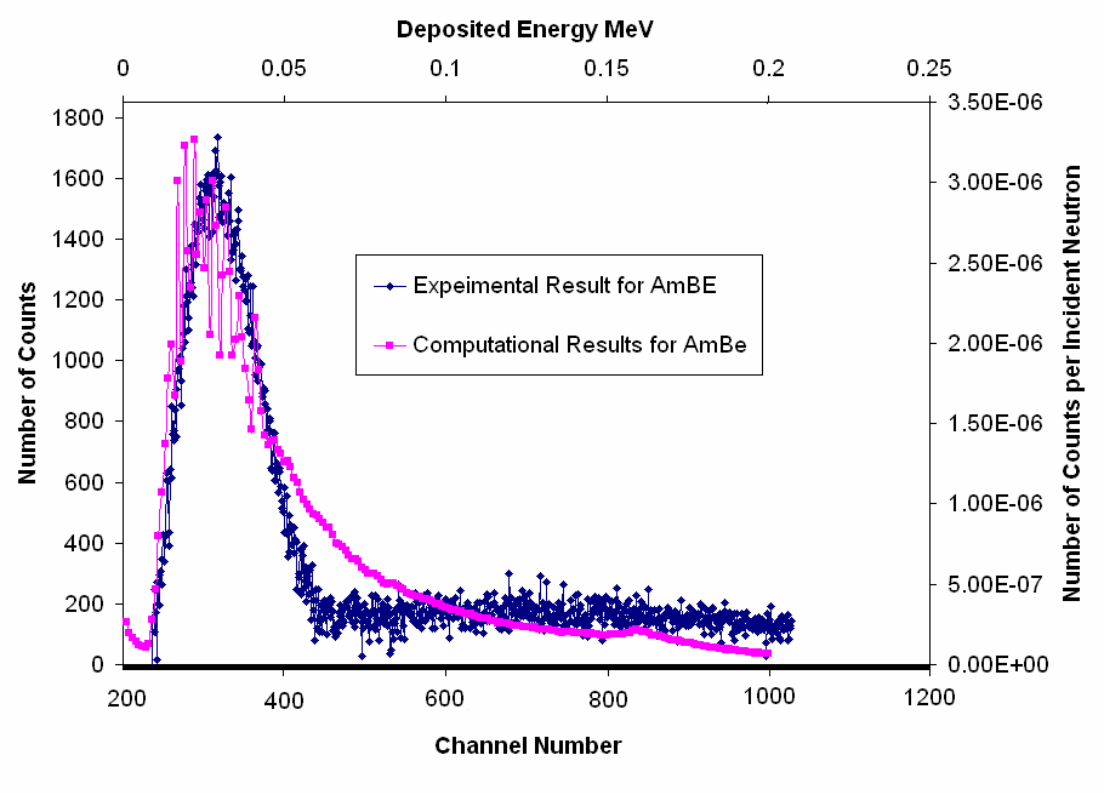

Figure 6.12. Comparison between the measured PHD and the simulated PHD of the AmBe neutrons.

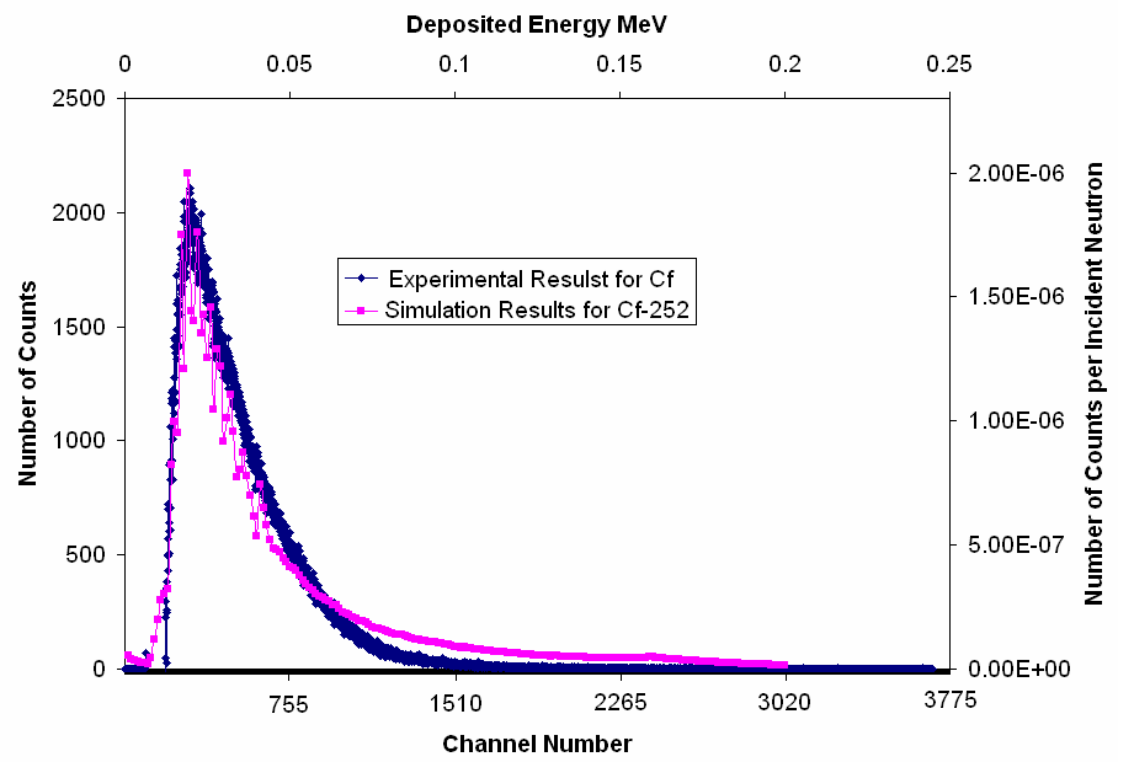

Figure 6.13. Comparison between the measured PHD and the simulated PHD of the ^{252}Cf neutrons.

CHAPTER 7
DISCUSSION

According to the experimental results presented in chapter 6, the optimal results were obtained when the GEM-based TEPC is operated with 1 atm of P-10 gas and with a bias voltage of 550 volts. The optimal results were judged based on the tradeoff between electron multiplication and energy resolution. It was noted, however, that even the optimal pulse height distributions shown in Figures 6.2 and 6.4 do not allow clean separations between neutron events and gamma-ray events. This presents a serious problem especially when the radiation field contains a large portion of gamma rays. The overlapping of the neutron events and gamma-ray events is mainly due to the large widths (2"×2") of the gas cavity. The large widths allow some of the electrons released via gamma-ray interactions to deposit as much or more energy as some protons released via neutron interactions. A straight forward way to overcome this problem, therefore, is to replace the single–cavity configuration by a multicavity configuration. Figure 7.1 shows the geometric configuration of a multicavity GEM-based TEPC. As shown in Figure 7.1(b), an electron entering the gas cavity at a glancing angle would likely be intersected by the Rexolite between two adjacent cavities, and therefore, will not be able to deposit much energy in the gas region. The trade-off of a multi-cavity detector, however, is a reduced neutron detection efficiency. This is because the neutron detection efficiency is directly proportional to the total cross section area of the gas cavities. As mentioned in Chapter 3, a simple way to increase neutron detection efficiency is to stack several GEM-based TEPC together in one unit. The detection efficiency is approximately proportional to the number of the TEPC. Figure 7.2 shows the design configuration of a device that consists of three GEM-based TEPCs stacked together. As shown, all three TEPCs share the same HV unit and preamplifier.

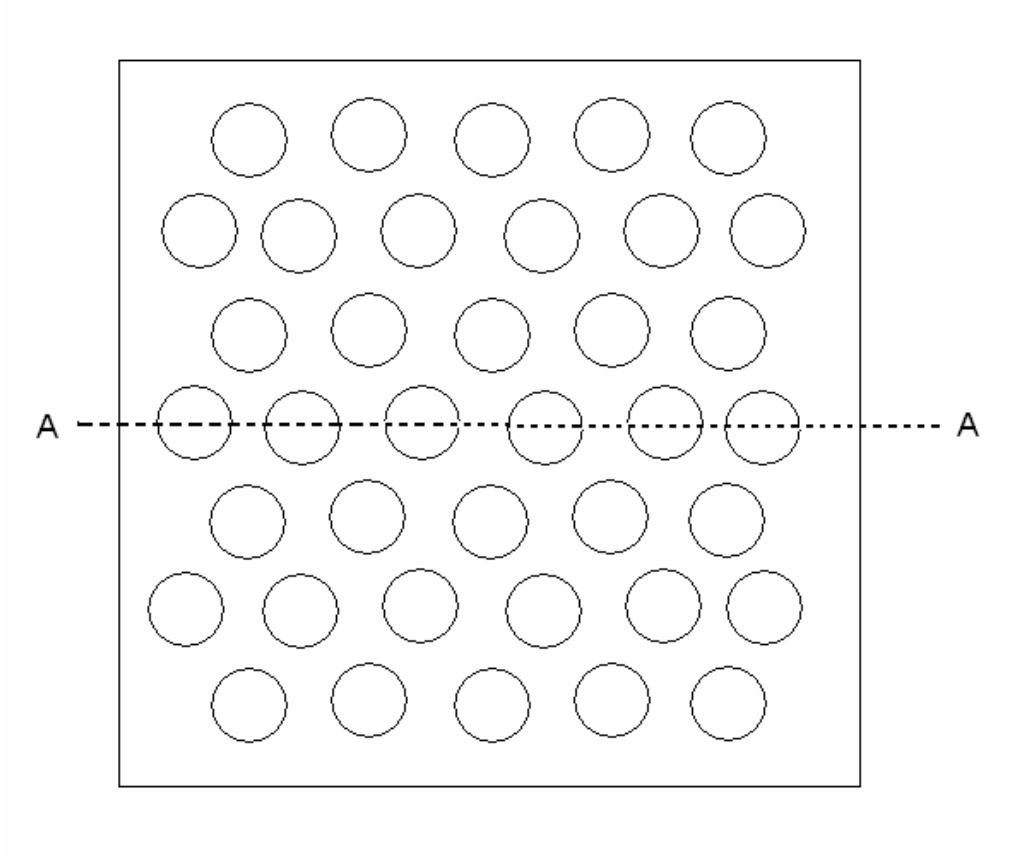

(a) Top view

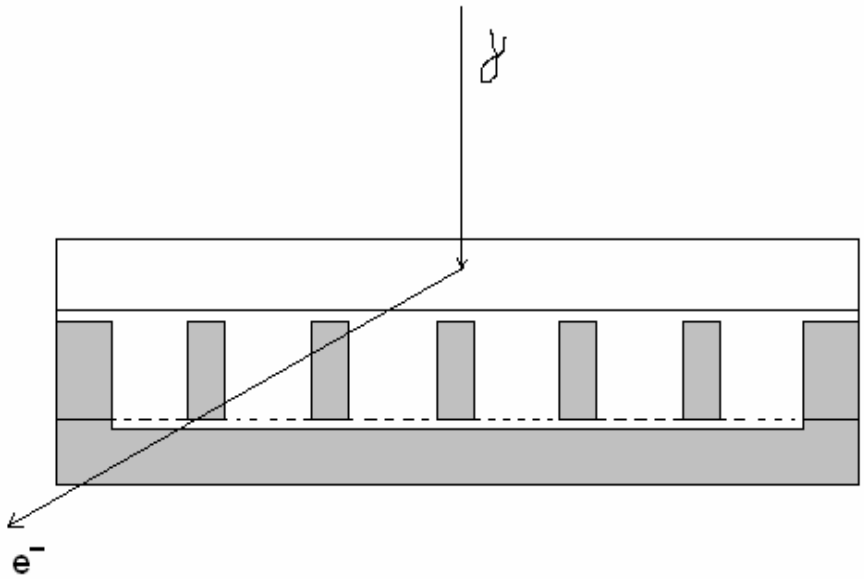

(b) XSEC view AA

Frigure 7.1. A multi-cavity GEM-based TEPC.

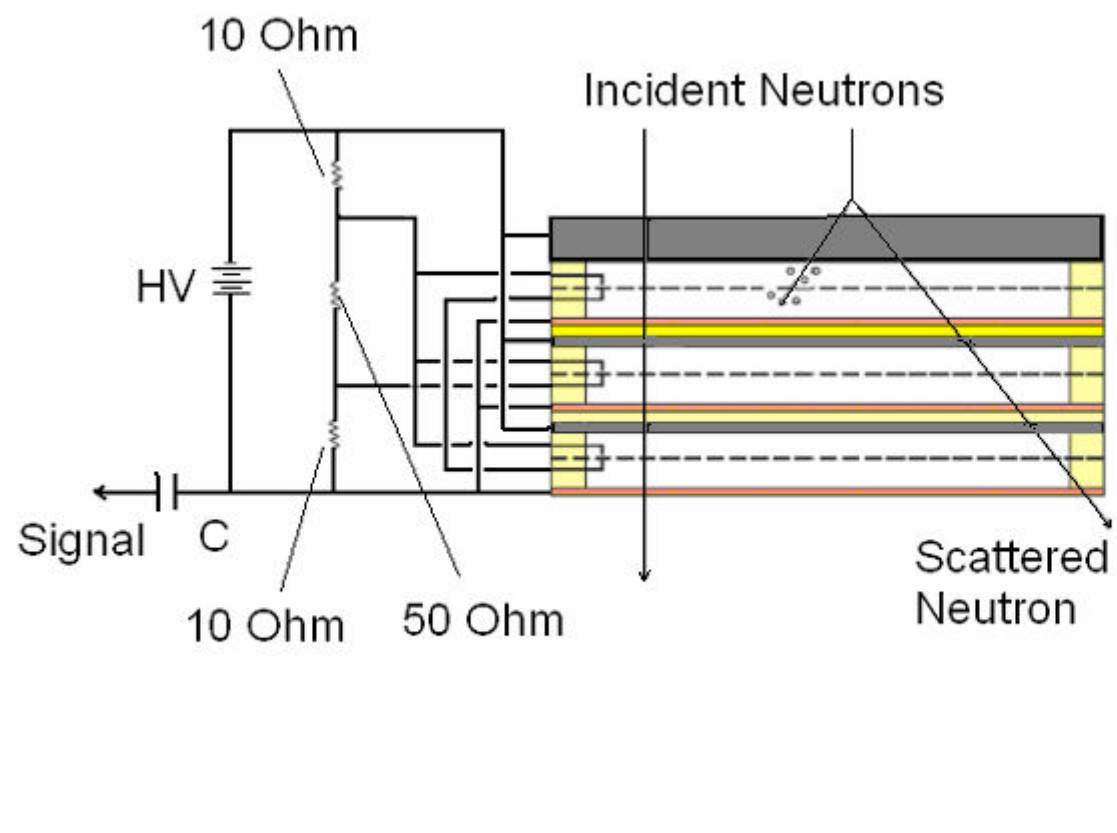

Figure 7.2. The design configuration of a device that consists of three GEM-based TEPCs.

One other problem of operating the GEM-based TEPC with 1 atm of P-10 gas is that the detector will not respond to neutrons with energies below 10 keV. To overcome this problem, one may mix 2/3 atm of P-10 gas with 1/3 atm of nitrogen to make a 1 atm mixed gas. As shown by the simulation results in chapter 4, 1/3 atm of nitrogen would produce enough events via $^{14}N(n,p)^{14}C$ reactions for low-energy neutrons and make the TEPC's neutron response curve closely resemble the $H^*(10)$ curve. The close resemblance between the TEPC's neutron response and the $H^*(10)$ curve, therefore, makes the GEM-based TEPC a neutron rem meter. Whether or not the mixed gas (i.e. 2/3 atm of P-10 and 1/3 atm of nitrogen) will work well as a proportional gas can only be known by conducting the experiments. The idea for choosing 1 atm as the total pressure for the mixed gas is based on practical considerations. In other words, a gas pressure of 1 atm would minimize gas leakage and thus eliminate the need of the gas flow system. This is an important requirement if the GEM-based TEPC is to be developed into a commercial neutron rem meter.

CHAPTER 8

CONCLUSIONS AND FUTURE WORK

Based on the study of this thesis the following conclusions can be drawn:

1. A GEM-based TEPC consisting of 2 inch×2 inch GEM, data acquisition system, and gas distribution system, was designed and constructed.
2. Monte Carlo simulations of the GEM-based TEPC were performed to determine the detector's response to neutrons and gamma rays. The Monte Carlo results show that a gas mixture of 1/3 atm P-10 and 1/3 atm nitrogen would make the TEPC's neutron response curve resemble the $H^*(10)$ curve.
3. The GEM-based TEPC was tested experimentally with two neutron sources (AmBe and ^{252}Cf) and one gamma-ray source (^{137}Cs). The experimental results agree well with the computational results, indicating that the GEM-based TEPC worked as expected.
4. The pulse height distributions obtained with the GEM-based TEPC do show that the pulse heights of neutron events are, in general, larger than those of gamma-ray events. However, separation between neutron events and gamma-ray events based on the PHDs is unsatisfactory.
5. Among the various gas types and gas pressures, 1 atm of P-10 gas gives the optimal results.

To further improve the performance of the GEM-based TEPC and make it a commercial neutron rem meter, the following recommendations are made for further work:

1. Build a new GEM-based TEPC with multiple gas cavities (see Figure 7.1) to allow better separations between neutron events and gamma-ray events.
2. Stack several GEM-based TEPCs together as one unit to increase the neutron events and gamma-ray events.
3. Place the detector unit in vacuum tight chamber and fill the detector with a gas mixture made of 2/3 atm of P-10 gas and 1/3 atm nitrogen. This would not only eliminate the use of gas flow system but also make the detector's neutron response curve mimic the $H^*(10)$ curve.

APPENDIX A

MONTE CARLO PROGRAM DESCRIPTION

A.1. FORTRAN Source Code

The following source code was used for the Monte Carlo simulation of the GEM-based TEPC described in the section 4.1

```
      DIMENSION EN1(101), PROB(101)
      DIMENSION EN2(21), SIG(21)
      DIMENSION EP(89), ARNG(89), PRNG(89)
      INTEGER DISTRB(200)
      COMMON /TABLE1/ EN1, PROB
      COMMON /TABLE2/ EN2, SIG
      COMMON /TABLE3/ EP, ARNG, PRNG
      OPEN (1, NAME = 'NPROB', STATUS = 'OLD')
      READ (1, 2) (EN1(I), PROB(I), I = 1,101)
    2 FORMAT (2(5X, E14.8))
      OPEN (2, NAME = 'SIGMAF', STATUS = 'OLD')
      READ (2, 3) (EN2(I), SIG(I), I = 1,21)
    3 FORMAT (2(5X, E14.8))
      OPEN (3, NAME = 'ipt', STATUS = 'OLD')
      READ (3, 4) (EP(I), ARNG(I), PRNG(I), I = 1,89)
    4 FORMAT (3(5x, E14.8))
      OPEN (4, NAME = 'OPTFNL')
C*************************************************************
C    INITIAL CONDITIONS
C
      N = 2000000000
C
C    *Zeroing DISTRB*
C
      NBIN = 200
      DO 5 I = 1,NBIN
          DISTRB(I) = 0
    5 CONTINUE
C
      EMAX = .2
      DIST = 1070.
      PROPD = 2000.
      IPENE = 0
      K = 0
   10 K = K + 1
      IF (K.EQ.N + 1) THEN
        GO TO 100
      ELSE
```

```
        GO TO 20
      END IF
C
C    *Determining energy of incoming neutron*
C
   20 ENPROB = RAND()
      CALL NEUTRN (ENPROB, ENN)
C
C    *Determining whether or not a neutron interacts*
C
      RNMBR = RAND()
      CALL SIGMAS (ENN, SIGMA)
      PROBOI = 1-EXP(-SIGMA*DIST)
      IF (RNMBR.LE.PROBOI) THEN
        GO TO 30
      ELSE
        GO TO 10
      END IF
C
   30 EPP = RAND()*ENN
      X = RAND()*DIST
      CT = SQRT(EPP/ENN)
      IF (CT.EQ.0.0) THEN
        GO TO 10
      ELSE
        GO TO 40
      END IF
C*************************************************************
C     FINDING INITIAL PROTON ENERGY
C
   40 CALL INTRP1 (EPP, ARANGE)
      R1 = ARANGE - (X/CT)
      IF (R1.LE.0.0) THEN
        GO TO 10
      ELSE
        GO TO 50
      END IF
   50 CALL INTRP2 (R1, EPPI)
C*************************************************************
C     FINDING TOTAL ENERGY DEPOSITED IN GAS BY ONE PROTON
C     AND THE # OF PROTONS THAT HAVE PENETRATED INTO THE GAS
C
      CALL INTRP3 (EPPI, PRANGE)
      R2 = PRANGE - (PROPD/CT)
      IF (R2.LE.0.0) THEN
        EDEPOS = EPPI
        IPENE = IPENE + 1
```

```
      ELSE
        CALL INTRP4 (R2, EPPF)
        EDEPOS = EPPI - EPPF
        IPENE = IPENE + 1
      END IF
C*************************************************************
C     TALLYING
C
      E = (NBIN/EMAX)*EDEPOS
      BIN = INT(E) + 1
      IF (BIN.GT.NBIN) THEN
        GO TO 10
      ELSE
        GO TO 90
      END IF
   90 DISTRB(BIN) = DISTRB(BIN) + 1
      GO TO 10
  100 WRITE (4,150) DISTRB
  150 FORMAT (3X, I10)
      WRITE (4, 200) IPENE
  200 FORMAT (3X, I10)
      END
C*************************************************************
C
      SUBROUTINE NEUTRN (ENPROB, ENN)
      DIMENSION EN1(101), PROB(101)
      COMMON /TABLE1/ EN1, PROB
      DO 20 I = 1,101
        IF (PROB(I).GE.ENPROB) THEN
          SLOPE = (EN1(I)-EN1(I-1))/(PROB(I)-PROB(I-1))
          YINT =EN1(I)-((EN1(I)-EN1(I-1))*PROB(I))/(PROB(I)-PROB(I-1))
          ENN = SLOPE*ENPROB + YINT
          GO TO 30
        ELSE
          GO TO 20
        END IF
   20 CONTINUE
   30 END
C*************************************************************
C
      SUBROUTINE SIGMAS (ENN, SIGMA)
      DIMENSION EN2(21), SIG(21)
      COMMON /TABLE2/ EN2, SIG
      DO 20 I = 1,21
        IF (EN2(I).GE.ENN) THEN
          SLOPE = (SIG(I)-SIG(I-1))/(EN2(I)-EN2(I-1))
          YINT = SIG(I)-((SIG(I)-SIG(I-1))*EN2(I))/(EN2(I)-EN2(I-1))
```

```
        SIGMA = SLOPE*ENN + YINT
        GO TO 30
      ELSE
        GO TO 20
      END IF
   20 CONTINUE
   30 END
C*************************************************************
C
      SUBROUTINE INTRP1 (EPP, ARANGE)
      DIMENSION EP(89), ARNG(89), PRNG(89)
      COMMON /TABLE3/ EP, ARNG, PRNG
      DO 20 I = 1,89
        IF (EP(I).GE.EPP) THEN
          SLOPE = (ARNG(I)-ARNG(I-1))/(EP(I)-EP(I-1))
          YINT =ARNG(I)-((ARNG(I)-ARNG(I-1))*EP(I))/(EP(I)-EP(I-1))
          ARANGE = SLOPE*EPP + YINT
          GO TO 30
        ELSE
          GO TO 20
        END IF
   20 CONTINUE
   30 END
C*************************************************************
C
      SUBROUTINE INTRP2 (R1, EPPI)
      DIMENSION EP(89), ARNG(89), PRNG(89)
      COMMON /TABLE3/ EP, ARNG, PRNG
      DO 20 I = 1,89
        IF (ARNG(I).GE.R1) THEN
          SLOPE = (EP(I)-EP(I-1))/(ARNG(I)-ARNG(I-1))
          YINT =EP(I)-((EP(I)-EP(I-1))*ARNG(I))/(ARNG(I)-ARNG(I-1))
          EPPI = SLOPE*R1 + YINT
          GO TO 30
        ELSE
          GO TO 20
        END IF
   20 CONTINUE
   30 END
C*************************************************************
C
      SUBROUTINE INTRP3 (EPPI, PRANGE)
      DIMENSION EP(89), ARNG(89), PRNG(89)
      COMMON /TABLE3/ EP, ARNG, PRNG
      DO 20 I = 1,89
        IF (EP(I).GE.EPPI) THEN
          SLOPE = (PRNG(I)-PRNG(I-1))/(EP(I)-EP(I-1))
```

```
        YINT =PRNG(I)-((PRNG(I)-PRNG(I-1))*EP(I))/(EP(I)-EP(I-1))
        PRANGE = SLOPE*EPPI + YINT
        GO TO 30
      ELSE
        GO TO 20
      END IF
   20 CONTINUE
   30 END
C*************************************************************
C
      SUBROUTINE INTRP4 (R2, EPPF)
      DIMENSION EP(89), ARNG(89), PRNG(89)
      COMMON /TABLE3/ EP, ARNG, PRNG
      DO 20 I = 1,89
        IF (PRNG(I).GE.R2) THEN
          SLOPE = (EP(I)-EP(I-1))/(PRNG(I)-PRNG(I-1))
          YINT =EP(I)-((EP(I)-EP(I-1))*PRNG(I))/(PRNG(I)-PRNG(I-1))
          EPPF = SLOPE*R2 + YINT
          GO TO 30
        ELSE
          GO TO 20
        END IF
   20 CONTINUE
   30 END
```

A.2. Table 'NPROB'

Table A2. Used in the program as 'NPROB,' lists neutron energies from 0-MeV to 10-MeV in the left column and corresponding y-values from the cumulative density function (cdf)* in the right

Neutron energy	y-values
0.00000000E+00	0.00000000E+00
0.10000000E+00	0.15557589E-01
0.20000000E+00	0.36482912E-01
0.30000001E+00	0.60836423E-01
0.40000001E+00	0.87537125E-01
0.50000000E+00	0.11585979E+00
0.60000002E+00	0.14527433E+00
0.69999999E+00	0.17537446E+00
0.80000001E+00	0.20583984E+00
0.89999998E+00	0.23641346E+00
0.10000000E+01	0.26688707E+00
0.11000000E+01	0.29709098E+00
0.12000000E+01	0.32688683E+00
0.13000000E+01	0.35616207E+00
0.14000000E+01	0.38482565E+00
0.15000000E+01	0.41280463E+00
0.16000000E+01	0.44004151E+00
0.17000000E+01	0.46649185E+00
0.18000000E+01	0.49212241E+00
0.19000000E+01	0.51690948E+00
0.20000000E+01	0.54083765E+00
0.20999999E+01	0.56389838E+00
0.22000000E+01	0.58608931E+00
0.23000000E+01	0.60741311E+00
0.24000001E+01	0.62787682E+00
0.25000000E+01	0.64749098E+00
0.25999999E+01	0.66626942E+00
0.27000000E+01	0.68422848E+00
0.28000000E+01	0.70138651E+00
0.29000001E+01	0.71776366E+00
0.30000000E+01	0.73338133E+00
0.30999999E+01	0.74826205E+00
0.32000000E+01	0.76242912E+00
0.33000000E+01	0.77590632E+00
0.34000001E+01	0.78871793E+00
0.35000000E+01	0.80088818E+00
0.35999999E+01	0.81244153E+00
0.37000000E+01	0.82340217E+00
0.38000000E+01	0.83379418E+00
0.39000001E+01	0.84364122E+00

0.40000000E+01	0.85296661E+00
0.40999999E+01	0.86179316E+00
0.41999998E+01	0.87014323E+00
0.43000002E+01	0.87803853E+00
0.44000001E+01	0.88550025E+00
0.45000000E+01	0.89254880E+00
0.45999999E+01	0.89920408E+00
0.46999998E+01	0.90548533E+00
0.48000002E+01	0.91141099E+00
0.49000001E+01	0.91699892E+00
0.50000000E+01	0.92226630E+00
0.50999999E+01	0.92722958E+00
0.51999998E+01	0.93190455E+00
0.53000002E+01	0.93630636E+00
0.54000001E+01	0.94044954E+00
0.55000000E+01	0.94434792E+00
0.55999999E+01	0.94801480E+00
0.56999998E+01	0.95146269E+00
0.58000002E+01	0.95470375E+00
0.59000001E+01	0.95774943E+00
0.60000000E+01	0.96061063E+00
0.60999999E+01	0.96329772E+00
0.61999998E+01	0.96582061E+00
0.63000002E+01	0.96818864E+00
0.64000001E+01	0.97041076E+00
0.65000000E+01	0.97249544E+00
0.65999999E+01	0.97445053E+00
0.66999998E+01	0.97628373E+00
0.68000002E+01	0.97800225E+00
0.69000001E+01	0.97961277E+00
0.70000000E+01	0.98112178E+00
0.70999999E+01	0.98253536E+00
0.71999998E+01	0.98385918E+00
0.73000002E+01	0.98509878E+00
0.74000001E+01	0.98625916E+00
0.75000000E+01	0.98734516E+00
0.75999999E+01	0.98836142E+00
0.76999998E+01	0.98931211E+00
0.78000002E+01	0.99020135E+00
0.79000001E+01	0.99103296E+00
0.80000000E+01	0.99181050E+00
0.81000004E+01	0.99253738E+00
0.81999998E+01	0.99321669E+00
0.83000002E+01	0.99385154E+00
0.83999996E+01	0.99444461E+00
0.85000000E+01	0.99499869E+00
0.86000004E+01	0.99551612E+00

0.86999998E+01	0.99599934E+00
0.88000002E+01	0.99645054E+00
0.88999996E+01	0.99687165E+00
0.90000000E+01	0.99726474E+00
0.91000004E+01	0.99763161E+00
0.91999998E+01	0.99797386E+00
0.93000002E+01	0.99829322E+00
0.93999996E+01	0.99859107E+00
0.95000000E+01	0.99886882E+00
0.96000004E+01	0.99912786E+00
0.96999998E+01	0.99936938E+00
0.98000002E+01	0.99959457E+00
0.98999996E+01	0.99980444E+00
0.10000000E+02	0.10000000E+01

A.3. Table 'SIGMAF'

Table A.3. Used as 'SIGMAF,' lists neutron energies from 0-MeV to 10-MeV in the left column and corresponding interaction cross-sections (Σ) with the unit μm^{-1} in the right

Neutron Energy(MeV)	Interaction Cross-Sections (Σ) (μm^{-1})
0.00000000E+00	0.14104000E-03
0.20000000E-01	0.12934400E-03
0.35999998E-01	0.12384000E-03
0.59999999E-01	0.11008000E-03
0.10000000E+00	0.96320000E-04
0.20000000E+00	0.68800000E-04
0.30000001E+00	0.55040000E-04
0.40000001E+00	0.48160000E-04
0.50000000E+00	0.42656000E-04
0.60000002E+00	0.37152000E-04
0.80000001E+00	0.32336000E-04
0.10000000E+01	0.28896000E-04
0.20000000E+01	0.19952000E-04
0.30000000E+01	0.15136000E-04
0.40000000E+01	0.12384000E-04
0.50000000E+01	0.11008000E-04
0.60000000E+01	0.96320000E-05
0.70000000E+01	0.86000000E-05
0.80000000E+01	0.79120000E-05
0.90000000E+01	0.68800000E-05
0.10000000E+02	0.63983998E-05

A.4. Table 'IPT'

Table A4. Referred to as 'ipt,' in the program. It lists proton energies from 0-MeV to 40-MeV in the left column, the proton range in A-150 with the unit μm in the middle, and the proton range in propane with the unit μm in the right.

Proton Energy (MeV)	Range in A-150(μm)	Range in propane(μm)
0.00000000E+00	0.00000000E+00	0.00000000E+00
0.10000000E-02	0.47142856E-01	0.58255814E+02
0.15000000E-02	0.65758653E-01	0.82500000E+02
0.20000001E-02	0.82431234E-01	0.10436047E+03
0.24999999E-02	0.97604260E-01	0.12428779E+03
0.30000000E-02	0.11153505E+00	0.14268895E+03
0.40000002E-02	0.13691215E+00	0.17601744E+03
0.49999999E-02	0.15971605E+00	0.20595930E+03
0.60000001E-02	0.18056788E+00	0.23328488E+03
0.70000002E-02	0.20000000E+00	0.25857559E+03
0.80000004E-02	0.21818988E+00	0.28226746E+03
0.89999996E-02	0.23540373E+00	0.30465115E+03
0.99999998E-02	0.25181898E+00	0.32587210E+03
0.12500000E-01	0.29006210E+00	0.37500000E+03
0.15000000E-01	0.32537711E+00	0.42049417E+03
0.17500000E-01	0.35856256E+00	0.46308139E+03
0.20000000E-01	0.39006212E+00	0.50319766E+03
0.22500001E-01	0.42014197E+00	0.54171509E+03
0.25000000E-01	0.44906834E+00	0.57848834E+03
0.27500000E-01	0.47710738E+00	0.61409882E+03
0.29999999E-01	0.50425911E+00	0.64869183E+03
0.35000000E-01	0.55669922E+00	0.71526166E+03
0.39999999E-01	0.60700977E+00	0.77906976E+03
0.45000002E-01	0.65572315E+00	0.84098834E+03
0.50000001E-01	0.70319432E+00	0.90145349E+03
0.55000000E-01	0.74968946E+00	0.96075580E+03
0.59999999E-01	0.79565215E+00	0.10194767E+04
0.64999998E-01	0.84117126E+00	0.10776163E+04
0.70000000E-01	0.88642412E+00	0.11356105E+04
0.75000003E-01	0.93167704E+00	0.11933140E+04
0.79999998E-01	0.97692990E+00	0.12513081E+04
0.85000001E-01	0.10221828E+01	0.13093024E+04
0.90000004E-01	0.10674356E+01	0.13677325E+04
0.94999999E-01	0.11126885E+01	0.14264535E+04
0.10000000E+00	0.11588287E+01	0.14854651E+04
0.12500000E+00	0.13957409E+01	0.17906976E+04
0.15000001E+00	0.16468500E+01	0.21162791E+04
0.17500000E+00	0.19148180E+01	0.24651162E+04
0.20000000E+00	0.22023070E+01	0.28401162E+04

0.22499999E+00	0.25084295E+01	0.32398257E+04
0.25000000E+00	0.28340728E+01	0.36671511E+04
0.27500001E+00	0.31783495E+01	0.41220933E+04
0.30000001E+00	0.35412600E+01	0.46061045E+04
0.34999999E+00	0.43203197E+01	0.56540698E+04
0.40000001E+00	0.51668143E+01	0.68110464E+04
0.44999999E+00	0.60771961E+01	0.80712207E+04
0.50000000E+00	0.70479150E+01	0.94316865E+04
0.55000001E+00	0.80798578E+01	0.10889535E+05
0.60000002E+00	0.91747999E+01	0.12440407E+05
0.64999998E+00	0.10346051E+02	0.14085756E+05
0.69999999E+00	0.11570541E+02	0.15813953E+05
0.75000000E+00	0.12874889E+02	0.17645350E+05
0.80000001E+00	0.14241348E+02	0.19563953E+05
0.85000002E+00	0.15678793E+02	0.21555232E+05
0.89999998E+00	0.17178350E+02	0.23633721E+05
0.94999999E+00	0.18740017E+02	0.25813953E+05
0.10000000E+01	0.20363798E+02	0.28066861E+05
0.12500000E+01	0.29352262E+02	0.40566859E+05
0.15000000E+01	0.39716061E+02	0.55058141E+05
0.17500000E+01	0.51419697E+02	0.71482555E+05
0.20000000E+01	0.64409935E+02	0.89767445E+05
0.22500000E+01	0.78669029E+02	0.10988372E+06
0.25000000E+01	0.94143745E+02	0.13178780E+06
0.27500000E+01	0.11091393E+03	0.15552325E+06
0.30000000E+01	0.12874889E+03	0.18081395E+06
0.35000000E+01	0.16805679E+03	0.23677325E+06
0.40000000E+01	0.21197870E+03	0.29927325E+06
0.45000000E+01	0.26042590E+03	0.36845931E+06
0.50000000E+01	0.31322095E+03	0.44389534E+06
0.55000000E+01	0.37027505E+03	0.52572675E+06
0.60000000E+01	0.43167703E+03	0.61380812E+06
0.65000000E+01	0.49733807E+03	0.70784881E+06
0.70000000E+01	0.56708075E+03	0.80813956E+06
0.75000000E+01	0.64090503E+03	0.91424419E+06
0.80000000E+01	0.71881097E+03	0.10264535E+07
0.85000000E+01	0.80070984E+03	0.11443314E+07
0.90000000E+01	0.88660162E+03	0.12681686E+07
0.95000000E+01	0.97604260E+03	0.13976744E+07
0.10000000E+02	0.10700977E+04	0.15334302E+07
0.12500000E+02	0.15962733E+04	0.22921512E+07
0.15000000E+02	0.22156167E+04	0.31889535E+07
0.17500000E+02	0.29254658E+04	0.42180235E+07
0.20000000E+02	0.37231589E+04	0.53750000E+07
0.22500000E+02	0.46069209E+04	0.66584300E+07
0.25000000E+02	0.55740903E+04	0.80654070E+07
0.27500000E+02	0.66237798E+04	0.95915700E+07

0.30000000E+02	0.77542148E+04	0.11236919E+08
0.35000000E+02	0.10248447E+05	0.14869186E+08
0.40000000E+02	0.13052352E+05	0.18968024E+08

APPENDIX B

MCNP INPUT FILES

Several examples of the MCNP input files are presented in the following section. The first input file is for the MCNP simulation with the detector filled with P-10 gas. The source is Cs-137 gamma source. The second input file is for the detector filled with the mixture of 1/3 atm P-10 gas with 1/3 atm of Nitrogen and monoenergetic neutron source.

B.1. Input File for GEM-based TEPC filled with P-10 gas, Cs-137 gamma source

```
Detector filled with P-10 and nitrogen
c gamma photons from Cs-137 spectrum calculation
1  1  -0.94      1 -2 -3 4 -5 6            $polyethylene
2  2  -1.127     7 -1 -3 4 -5 6            $A-150
3  3  -0.00155   8 -7 -3 4 -5 6            $p-10 gas cell
4  0           -8 : 2 : 3 : -4 : 5 : -6    $void
c end of cel cards

c surfaces
1  PZ  -1                        $bottom plane
2  PZ   1                        $top plane
3  PY   5                        $right plane
4  PY  -5                        $left plane
5  PX   5                        $front plane
6  PX  -5                        $back plane
7  PZ  -1.2                      $bottom of A-150
8  PZ  -1.6                      $bottom of a p10 gas cell

c data cards
MODE P E
IMP:P,E 1 1 1 0
SDEF SUR=2 NRM=-1 ERG=0.661 PAR=2          $Cs-137 gamma source
*F8:E 3                          $energy distribution of pulses in p10 gas cell 3
E8:E  1.0E-4 2.0E-4 3.0E-4 4.0E-4 5.0E-4
      6.0E-4 7.0E-4 8.0E-4 9.0E-4 1.0E-3
      2.0E-3 3.0E-3 4.0E-3 5.0E-3 6.0E-3
      7.0E-3 8.0E-3 9.0E-3 10.0E-3 11.0E-3
      12.0E-3 13.0E-3 14.0E-3 15.0E-3 16.0E-3
      17.0E-3 18.0E-3 19.0E-3 20.0E-3 21.0E-3
      22.0E-3 23.0E-3 24.0E-3 25.0E-3 26.0E-3
      27.0E-3 28.0E-3 29.0E-3 30.0E-3 31.0E-3
      32.0E-3 33.0E-3 34.0E-3 35.0E-3 36.0E-3
      37.0E-3 38.0E-3 39.0E-3 40.0E-3 41.0E-3
      42.0E-3 43.0E-3 44.0E-3 45.0E-3 46.0E-3
```

```
     47.0E-3 48.0E-3 49.0E-3 50.0E-3 51.0E-3
     52.0E-3 53.0E-3 54.0E-3 55.0E-3 56.0E-3
     57.0E-3 58.0E-3 59.0E-3 60.0E-3 61.0E-3
     62.0E-3 63.0E-3 64.0E-3 65.0E-3 66.0E-3
     67.0E-3 68.0E-3 69.0E-3 70.0E-3 71.0E-3
     72.0E-3 73.0E-3 74.0E-3 75.0E-3 76.0E-3
     77.0E-3 78.0E-3 79.0E-3 80.0E-3 81.0E-3
     82.0E-3 83.0E-3 84.0E-3 85.0E-3 86.0E-3
     87.0E-3 88.0E-3 89.0E-3 90.0E-3 91.0E-3
     92.0E-3 93.0E-3 94.0E-3 95.0E-3 96.0E-3
     97.0E-3 98.0E-3 99.0E-3 100.0E-3 101.0E-3
     102.0E-3 103.0E-3 104.0E-3 105.0E-3 106.0E-3
     107.0E-3 108.0E-3 109.0E-3 110.0E-3 111.0E-3
     112.0E-3 113.0E-3 114.0E-3 115.0E-3 116.0E-3
     117.0E-3 118.0E-3 119.0E-3 120.0E-3 121.0E-3
     122.0E-3 123.0E-3 124.0E-3 125.0E-3 126.0E-3
     127.0E-3 128.0E-3 129.0E-3 130.0E-3 131.0E-3
     132.0E-3 133.0E-3 134.0E-3 135.0E-3 136.0E-3
     137.0E-3 138.0E-3 139.0E-3 140.0E-3 141.0E-3
     142.0E-3 143.0E-3 144.0E-3 145.0E-3 146.0E-3
     147.0E-3 148.0E-3 149.0E-3 150.0E-3 151.0E-3
     152.0E-3 153.0E-3 154.0E-3 155.0E-3 156.0E-3
     157.0E-3 158.0E-3 159.0E-3 160.0E-3 161.0E-3
     162.0E-3 163.0E-3 164.0E-3 165.0E-3 166.0E-3
     167.0E-3 168.0E-3 169.0E-3 170.0E-3 171.0E-3
     172.0E-3 173.0E-3 174.0E-3 175.0E-3 176.0E-3
     177.0E-3 178.0E-3 179.0E-3 180.0E-3 181.0E-3
     182.0E-3 183.0E-3 184.0E-3 185.0E-3 186.0E-3
     187.0E-3 188.0E-3 189.0E-3 190.0E-3 191.0E-3
     192.0E-3 193.0E-3 194.0E-3 195.0E-3 196.0E-3
     197.0E-3 198.0E-3 199.0E-3 200.0E-3 201.0E-3                $separation by energy
c material cards
M1 1001 2    6000 1                                                          $polyetylene
M2 1001 -0.101327 6000 -0.775501  7014.42c -0.035057 8016.21c -0.052316 $A-150
M3 18000 -0.95 6000 -0.03 1001 -0.02                                         $P-10 gas
NPS 100000000
```

B.2. MCNP Input File for P-10 gas mixed with nitrogen

```
c GEM-based TEPC with 1/3 atm of P-10 and 1/3 atm of nitrogen
1  1  -0.94          1 -2 -3 4 -5 6          $polyethylene
2  2  -1.127         7 -1 -3 4 -5 6          $A-150
3  3  -0.000917      8 -7 -3 4 -5 6          $P-10+Nitrogen cell
4  0           -8 : 2 : 3 : -4 : 5 : -6       $void
c end of cel cards

c surfaces
1  PZ  -1                        $bottom plane of polyethylene
2  PZ   0                        $top plane
3  PY   5                        $right plane
4  PY  -5                        $left plane
5  PX   5                        $front plane
6  PX  -5                        $back plane
7  PZ  -1.2                      $bottom of A-150
8  PZ  -1.5                      $bottom of a P-10/nitrogen cell

c data cards
IMP:N 1 1 1 0
SDEF SUR=2 NRM=-1 ERG 1.0E-7                  $source on the surface
F6:N 3                          $energy deposited averaged over a P-10/nitrogen cell 3
E6:N  1.0E-8 2.0E-8 3.0E-8 4.0E-8 5.0E-8 6.0E-8 7.0E-8
     8.0E-8 9.0E-8 1.0E-7       $separation by energy
F2:N 1                          $flux across the surface 1
E2:N  1.0E-8 2.0E-8 3.0E-8 4.0E-8 5.0E-8 6.0E-8 7.0E-8
     8.0E-8 9.0E-8 1.0E-7       $separation by energy
c material cards
M1 1001 2    6000 1                                                    $polyetylene
M2 1001 -0.101327 6000 -0.775501  7014.42c -0.035057 8016.21c -0.052316 $A-150
M3 18000.35c 150.2 6000.50c 5.6 1001.35c 1.9 7014 72.4                  $ P-10+Nitrogen
                                    NPS 10000000
```

REFERENCES

[1] ICRP, "Recommendations of the International Commission on Radiological Protection," Publication 26, Pergamon Press 1977.

[2] ICRP, "Recommendations of the International Commission on Radiological Protection," Publication 60, Pergamon Press 1991.

[3] ICRU "Determination of Dose Equivalents Resulting from External Radiation Sources – Part 2," Report 39, ICRU publications 1985.

[4] ICRU "Determination of Dose Equivalents Resulting from External Radiation Sources – Part 2," Report 43, ICRU publications 1988.

[5] ICRU International Commission on Radiation Units and Measurements, "Neutron Dosimetry for Biology and Medicine," Report 26, ICRU publications 1977.

[6] Farahmand, M., Bos, A.J. and van Eijk, C.W.E. Gas Electron Multiplier (GEM) operation with tissue-equivalent gases at various pressures. *Nuclear Instruments And Methods* A 506, 160-165 (2003)

[7] Cember. Introduction to Health Physics. Pergamon Press, New York, 1983

[8] IAEA. Basic Requirements for Personnel Monitoring. Technical Report Safety Series No.14, International Atomic Energy Agency, 1965

[9] IAEA and Who. Basic Requirements for Personnel Monitoring. Technical Report STI/PUB/599, International Atomic Energy Agency, 1980

[10] G. Cowper. The New Operational Quantities for Radiation Protection Recommended by the ICRU: Various Practical Considerations. *Radiation Protection Dosimetry,* 12(2), 159-162, 1985

[11] G. Burger, A. Morhart, and A. Wittmann. The Conceptual Basis for Neutron Radiation Protection. In H. Schraube, G. Burger, and J. Booz, editors, Proceedings of the Fifth Symposium on Neutron Dosimetry, 71-86, Luxembourg, 1984. Commission of the European Communities.

[12] ICRP. Recommendations of the International Commission on Radiological Protection. Technical Report 26, International Commission on Radiological Protection, 1977

[13] T. Burlin. Current Concepts in Radiation Protection. In G. Burger and H.G. Ebert, editors, Proceedings of the Fourth Symposium on Neutron Dosimetry, 15-31, Brussels, 1981. Commission of the European Communities.

[14] W.G Gross and H. Ing. Quality Factors for Monoenergetic Neutrons. *Radiation Research*, 99, 1-19, 1984.

[15] ICRP. 1990 Recommendations of the International Commission on Radiological Protection. Technical Report 60, International Commission on Radiological Protection, 1991

[16] ICRU. Determination of Dose Equivalents Resulting form External Radiation Sources. Technical Report 39, International Commission on Radiation Units and Measurements, 1985.

[17] B.R. Siebert and H. Schuhmacher. Calculated Fluence-to-Directional and Personal Dose Equivalent Conversion Coefficients for Neutrons. *Radiation Protection Dosimetry,* 54(3/4), 231, 1994

[18] B.R. Siebert and H. Schuhmacher. Quality Factors, Ambient and Personal Dose Equivalent for Neutrons, Based on the New ICRU Stopping Power Data for Protons and Alpha Particles. *Radiation Protection Dosimetry*, 58(3), 177, 1995.

[19] B.R. Siebert and H. Schuhmacher. Quality Factors, Ambient and Personal Dose Equivalent for Neutrons, Based on the New ICRP Stopping Power Data for Protons and Alpha Particles. *Radiation Protection Dosimetry*, 40(2), 85-89, 1992.

[20] G. Leuthold, V. Mares, and H. Schraube. Calculation of the Neutron Ambient Dose Equivalent on the Basis of the ICRP Revised Quality Factors. *Radiation Protection Dosimetry*, 40(2), 77-84, 1992.

[21] J.R. Harvey and A.J. Mill. A proposed Procedure for Standardizing the Relationship Between Ambient Dose Equivalnet And Neutron Fluence. *Radiation Protection Dosimetry,* 12(2), 141-143, 1985

[22] S.R. Wagner, B. Grosswendt, A.J.Mill J.R. Harvey, H.J. Selbach and B.R.L. Siebert. Unified Conversion Functions for the New ICRU Operational Radiation Protection Quantities. *Radiation Protection Dosimetry*, 12(2), 231-235, 1985

[23] ICRP Publication 74: Conversion Coefficients for use in Radiological Protection against External Radiation, International Commission of Radiological Protection, 1997

[24] R.E. Apfel. Detector and Dosimeter for Neutrons and Other Radiations. Technical Report 4143274, U.S. Patent, 1979

[25] R.E. Apfel et al. Superheated Drop Detector: A Possible Alternative for Neutron Dosimetry. *Radiation Protection Dosimetry*, 10, 327, 1985

[26] ICRU. The Quality factor in radiation protection. Report 40, International Commission on Radiation Units and Measurements, 1986

[27] Data sheet for HPI REM 500, Far West Technology, Inc., http://www.fwt.com

[28] S. Bachman, A. Bressan, L. Ropelewski, F. Sauli, D. Mormann, Recent progress in GEM manufacturing and operation. *Nuclear Instruments and Methods A,* 433, 464, 1999

[29] F. Sauli, "GEM: A new concept for electron amplification in gas detectors, "*Nuclear Instruments And Methods A*, .386, 531-534, 1997

[30] F. Sauli, S. Kappler, and L. Ropelewski, Electron Collection and Ion Feedback in GEM-Based detectors *IEEE Transactions on Nucler Science* 50*,* 803-808, 2003

[31] R. Chechik, A. Breskin, G. Garty, J. Mattout, F. Sauli, E. Shefer. First results on the GEM operated at low gas pressures, *Nuclear Instruments and Methods A*. 419, 423, 1998

[32] M. Capeans, B. Ketzer, A. Placci, L. Ropelewski, F. Sauli, M. van Steins. Construction of GEM Detectors for the Compass Experiment. Technical Note, CERN-EP/TA1, 2001

[33] J. Breimeister. Monte Carlo N-Particle Transport Code System. Los Alamos National Laboratory, 4A edition, 1994. MCNP4A code manual distributed through the RSIC computer code collection.

[34] D. Bogart, D.F. Shook, D. Fieno. Transport Analysis of Measured Neutron Leakage Spectra form Spheres as Tests of Evaluated High-Energy Cross Sections. *Nuclear Science and Engineering*. 53, 285-303, 1974.

[35] R. H. Olsher, D. T. Seagraves, S. L. Eisele, C. W. Bjork, W. A. Martinez, L. L Romero, M. W. Mallett, M. A. Duran, C. R. Hurlbut, PRESCILA: A new, lightweight neutron rem meter. *Health Phys*. 86, no. 6, 603-612. 2004.

[36] R.L. Bramblett, R.I. Ewing, T.W. Bonner. A New Type of Neutron Spectrometer. *Nuclear Instruments and Methods A*, 9, 1-12. 1960

[37] I.O. Andersson, J.A. Braun. A Neutron Rem Counter With Uniform Sensitivity form 0.025 ev to 10 MeV. Neutron Dosimetry. 2., proceedings of an International Atomic Agency Symposium. Vienna. 87-95, 1963

[38] M. Farahmand, A.J.J. Bos, C.W.E. van Eijk. Gas electron multiplier (GEM) operation with tissue-equivalent gases at various pressures. *Nuclear Instruments and Methods in Physics Research A* 506 160-165 2003

[39] G.F. Knoll, Radiation Detection and measurements. Wiley, New York, 1999

[40] S. Gerdung, P. Pihet, J.E. Grindborg, H. Roos, U.J. Schrewe, H. Schuhmacher.

Operation and Application of Tissue-Equivalent Proportional Counter. *Radiation Protection Deosimetry*. 61, 381 1995